COMPUTER SIMULATION OF THERMAL-HYDRAULICS OF MNSR FUEL-CHANNEL ASSEMBLY USING LabVIEW

By

LEONARD ALELE GADRI

(10363740)

BSc. Mathematics (KNUST), 1990

This thesis is submitted to the University of Ghana, Legon in partial fulfillment of the requirement for the award of MPhil Computational Nuclear Sciences and Engineering Degree

JULY, 2013

DECLARATION

I hereby declare that with the exception of references to other people work which have duly been acknowledged, this compilation is the result of my own research work and no part of it has been presented for another degree in this university or elsewhere.

……..

LEONARD ALELE GADRI

(Candidate)

Date……

I hereby declare that the preparation of this project was supervised in accordance with guidance of the supervision of Thesis work laid down by the University of Ghana.

…….. ……. ……

Prof. EDWARD AKAHO **NANA (Prof.) A. AYENSU GYEABOUR I.**

(PRINCIPAL SUPERVISOR) (Co-SUPERVISOR)

Date…… Date……

DEDICATION

To my children James Nutifafah, Belinda, Brenda, Yayra and Makafui for their support and prayers.

ACKNOWLEDGEMENT

I thank Jehovah for His favor, love and mercy which have enabled me to come out with this work.

My sincere thanks go to all the Lecturers in the Department of Nuclear Engineering, more especially to my supervisors Nana (Prof.) A. Ayensu Gyeabour I and Prof. E. H. K. Akaho whose efforts and support have brought this research work to fruition.

I dearly recall my course mates, particularly, Mr. Justice Darko, Mr. Robert Nunoo and Mr. Joseph Djangmah for their advice and support.

I deem it fit to put on record the advice of my predecessors: Mr. Alex Akoto Danso, Miss Rita Appiah and Mr. Emmanuel Proven Adzri towards the preparation of this work.

TABLE OF CONTENTS

LIST OF TABLES

LIST OF FIGURES

LIST OF SYMBOLS AND CONSTANTS

Symbol	Meaning	Units
σ_f(E)	Fission cross-section as a function of neutron Energy.	barns
Φ(r,z)	Neutron flux as a function of neutron Energy	neutrons/cm^3
N_f	Number of fissile atoms per unit volume	atoms/cm^3
q''' (r)	Volumetric heat generation	MW/m^3
Σ_f(E)	Macroscopic fission cross-section	barns
J_o	Zero order Bessel function of first kind	
J_1	First order Bessel function of first kind	
q_0'''	Maximum heat generation rate within reactor	kW
P_t	Total power of the reactor	kW
P_C	Total fuel Channel Power	kW
λ	Mean free path in the gas	m
h_{con}	Total conductance	W/m^2°C
q'	Heat flux	kW/m^2°C
Q	Power density	W/m^3
q''	Heat transfer	W/m^2°C
r_f	Radius of fuel	m
r_c	Radius of cladding	m
z	Axial height	m
μ	Viscosity of the gas	Ns/m^2
V	Volume of the reactor core	m^3
h_g	Gap conductance	W/m^2°C
$\acute{m}$	Mass flow rate	kg/s
T	Temperature (or temperature of the coolant)	°C

τ	time	s
h_c	Convective heat transfer	W/m^2 ℃
C	Specific heat	J/kg
ρ_f	Specific mass of fuel	kg/m^3
ρ_c	Specific mass of cladding	kg/m^3
σ	Stefan-Boltzman constant	
T_o	Temperature of fuel center line	℃
T_f	Temperature of fuel surface in axial	
	(or in the fuel in the radial) directions	℃
T_c	Temperature at outer surface of fuel	℃
T_d	Temperature in the cladding in the radial direction	℃
T_h	Temperature in the coolant in the radial direction	℃
k_f	Thermal conductivity of the fuel	W/m ℃
k_c	Thermal conductivity of the of the cladding	W/m ℃

LIST OF ABBREVIATIONS

AP 1000	Westinghouse AP 1000 (Advanced Passive) Nuclear Reactor
GHARR-1	Ghana's Research Reactor 1
LabVIEW	Laboratory Virtual Instrumentation Engineering Workbench
MATLAB	Matrix Laboratory
MNSR	Miniature Neutron Source Reactor
PC	Personal Computer

ABSTRACT

A LabVIEW simulator of thermal hydraulics has been developed to demonstrate the temperature profile of coolant flow in the reactor core during normal operation. The simulator could equally be used for any transient behavior of the reactor.

Heat generation, transfer and the associated temperature profile in the fuel-channel elements viz: the coolant, cladding and fuel were studied and the corresponding analytical temperature equations in the axial and radial directions for the coolant, outer surface of the cladding, fuel surface and fuel center were obtained for the simulation using LabVIEW.. Tables of values for the equations were constructed by MATLAB and Excel software programs. Plots of the equations with LabVIEW were verified and validated with the graphs drawn by the MATLAB.

In this thesis, an analysis of the effects of the coolant inlet temperature of 24.5 ℃ and exit temperature of 70.0 ℃ on the temperature distribution in fuel- channel elements of the reactor core of cylindrical geometry was carried out. Other parameters, including the total fuel channel power, mass flow rate and convective heat transfer coefficient were varied to study the effects on the temperature profile. The analytical temperature equations in the fuel channel elements of the reactor core were obtained. MATLAB and Excel software were used to construct data for the equations. The plots by MATLAB were used to benchmark the LabVIEW simulation. Excellent agreement was obtained between the MATLAB plots and the LabVIEW simulation results with an error margin of 0.001.

The analysis of the results by comparing gradients of inlet temperature, total reactor channel power and mass flow indicated that inlet temperature gradient is one of the key parameters in determining the temperature profile in the MNSR core.

CHAPTER ONE

INTRODUCTION

1.1 Background of the research

Nuclear power reactor produces nuclear energy in a controlled manner. Nuclear reactors are used for either research or power production. A power reactor is designed to produce heat for use in driving steam turbines to generate electricity. A research reactor is designed to produce beams of radiation for experimental applications. The heat produced is a waste product and is dissipated as proficiently as possible by the coolant.

Since the nuclear energy renaissance, there has been a mounting interest for nuclear professionals which in turn has given rise to the creation of nuclear science and engineering education programs at universities in a number of countries, including Ghana. The increase in the number of students undergoing nuclear degrees at the various levels need deeper understanding of the phenomena in connection with nuclear fission by way of simulation in other to assist in their education and training endeavors.

A reactor is an enormously complex machine. A number of things can go wrong with the reactor undetected. One malfunction will lead to another and then to a series of others until the core of the reactor begins to melt. A highly trained nuclear engineer may not know how to respond by way of putting the situation under control. [1]

In nuclear reactors, the fission is the origin of the thermal energy generation and much smaller source comes from non-fission process due to neutron capture in the fuel,

coolant, moderator and structural materials. The coolant affects significantly, the operating temperature and pressure, the size of the core, and methods of fuel handling. The thermal energy released in the fuel rods is transferred by heat conduction to the surface of the rod and then by convection to the coolant which circulates around the rods. In the process, the coolant transports the thermal energy released by fission in the reactor to external heat exchangers called steam generators of nuclear reactors.

Research reactor has received much attention in recent years due to its redesign and installation in a number of countries which wanted to supplement their power supply by nuclear power in future. Research reactor has many uses and building research reactor has also been investigated as a potential start of building power reactors.

Thermal-hydraulics are computed on the basis of a one or multidimensional core description. Lumped parameters models for thermal-hydraulics were generally considered only for qualitative studies of reactor dynamics. In these simplified models temperature effects were accounted for through a single effective temperature for the whole core. The temperature effects were described by considering four distinct temperature regions, corresponding respectively to the coolant, outer surface of cladding, fuel surface and fuel center.

This enables reactivity feedback to include all the major contributions, namely, moderator temperature effects, cladding temperature effects and fuel temperature effects. In line with the point model concept, coolant, clad and fuel temperatures were assumed to be functions separable in space and time. The space dependence was postulated to be the static distribution corresponding to a one-dimensional (in the axial direction) core.

1.2. Research Problem Statement

Computer simulation of the temperature profile in the coolant, clad and the fuel of an MNSR was undertaken in order to examine and visualize the thermal-hydraulics of the nuclear reactor by LabVIEW development platform, which was later validated by MATLAB and Excel programs.

Nuclear reactor is in fact one of the most sophisticated and complex systems man has ever made which is associated with very high risks due to nuclear fission.

Considering the immense uses and benefits of nuclear reactors which outweighed the risks, it has become very essential to have in depth understanding of the behavior of the reactor core during operation and of the technological solutions inherent in the thermal design of nuclear reactors.

1.3. Justification of the Research Project

A number of countries including Ghana, in their energy policy plan to adopt nuclear energy has taken giant steps towards operating research reactors, as a starting point in acquiring nuclear power plants. The GHARR-1 MNSR research reactor has been well managed and researches have been conducted to acquire knowledge and monitor the operations. Critical research has been on thermal-hydraulics, both engineering and analytical and numerical computations. The present research dealt with computer simulations of thermal-hydraulics which would serve as teaching and learning simulator.

Apart from this research being used as a teaching and learning aid, more can be learnt of the temperature distribution in the reactor core which can:

(a) keep alive the proposal by the government of Ghana to install nuclear power plant by the year 2020.

(b) bring about the awareness of technological solutions of nuclear reactor challenges to ward off fear.

(c) make this civilized idea of going nuclear by 2020 a reality and give it further impetus.

Besides, though extensive research has been carried out on the temperature profile in the reactor core, investigation revealed that LabVIEW has not been applied to simulate the temperature distribution in the components of the reactor core.

1.4. Research Aims and Objectives.

The main aim of this research was to simulate the mathematical models for the temperature distribution in the components of the MNSR fuel channel assembly by using LabVIEW development platform.

The objectives were to:

(a) find out, whether or not the proposed temperature changes in the fuel-channel elements will put the operation of the reactor outside the operational limits and conditions.

(b) state the rate of heat generation and removal in relation to possibility of overheating or insufficient cooling.

(c) predict the behavior of the research reactor.

(f) train reactor operators and students in nuclear reactor systems using this research simulator for teaching and learning methodology.

1.5. Scope of Research.

The research reactor type whose fuel rods are placed in channels which run through the reactor core is considered. The coolant circulates around the rods. The reactor core is cylindrical in shape and surrounded by lateral and axial reflectors. The reflectors prevent the leaking neutrons from escaping but return them to the reactor core.

To enable the prediction of the behavior of reactor core it requires a sound knowledge of the temperature distribution in the reactor fuel channel assembly during the steady state and transient conditions. Consequently, the temperature distributions in the radial and axial directions in the cylindrical fuel element are considered but for steady state conditions only.

1.6. Organization of the Thesis.

The thesis is organized in the following way. The first Chapter presents the background, justification and the objectives of the research. Chapter 2 describes the literature review. Chapter 3 illustrates the research methodology. Detailed results and discussions are dealt with in chapter 4. Finally, the conclusions and recommendations are summarized in chapter 5.

CHAPTER TWO

LITERATURE REVIEW

A large number of researches have been carried out on the thermal-hydraulics and heat generation studies of nuclear reactor cores.

2.1 Generation of heat in nuclear reactors

2.1.1. Thermal energy release during fission

The thermal energy released during fission is mainly due to fission process and much smaller amount due to non-fission neutron capture in the fuel, moderator, coolant and structural materials [2]

A total of about 207 Mev of energy is emitted during fission. The distribution of this energy among different components of a neutron-induced fission of U-235 is shown in Table 2.1 which also includes the energy converted into heat or the recoverable energy. Apparently, the emitted energy and the recoverable energy are not the same. This is due to the fact that for the total emitted energy during the fission process, the kinetic energy of the fission fragments, neutrons, gammas and betas are converted into heat in the reactor core and shielding materials while the neutrinos which accompany β-decay escape from the reactor virtually without any interaction .

Table 2.1. Emitted and recoverable energies for fission of ^{235}U [2].

Components	Emitted Energy	Energy Converted to heat or recovered energy	
	Mev	Mev	% of total
Fission fragments	168	168	84
Neutrons	5	5	2.5
Prompt γ rays	7	7	3.5
Delayed radiations:			
B-rays	8	8	4
γ-rays	7	7	3.5
Neutrinos	12	-	-
Capture γ-rays	-	5	2.5
TOTAL	207	200	100

Moreover, a new item which consists of capture γ-rays has been created. The capture γ-rays or radioactive capture reactions account for (v-1) neutrons per fission (v is the average number of neutrons emitted per fission; v is approximately equal to 2.5 for U-235) which are absorbed in the reactor without producing any fission reaction.

About 3 to 12 Mev of capture γ-radiation is produced per fission. An average value of 5 Mev is included in Table 2.1 and all this γ-ray is recoverable for the reactor system.

2.1.2 Analysis of energy converted to heat.

Nearly 84 % and 4 % of the energy converted to heat are due to the fission fragments and to the β-rays, respectively. The very short range of fission fragments: 10^{-2} mm from the fission site and β-rays less than 1mm ensures that this heat release takes place within the fuel elements. The energy release during neutron thermalization takes place in the moderator. The energy release due to neutron capture occurs largely

within the fuel and a small portion of this energy is released in the structural material, in the moderator and in the coolant as shown in Table 2. 1.

2.1.3 Heat distribution among the different reactor components

In line with the thermal design of nuclear reactors, it can be assumed that 94 % of the fission energy release takes place in the in the fuel, 5.2 %, 0.6 % and 0.3 % in the moderator, coolant and shielding respectively of an MNSR as illustrated in Table 2.2

Table 2.2 Distribution of heat release among different components in a research reactor [2]

Component	**Released Thermal Energy, %**
Energy Released in fuel	93.9
Energy Released in coolant	0.6
Energy released in moderator	5.2
Energy released in the Shielding	0.3
Total	100.0

2.1.4 Volumetric heat generation rate in reactor fuel

Given fission cross-section as a function of the neutron energy, $\sigma_{f(E)}$, the neutron flux as a function of the neutron energy and space $\phi(\vec{r}, E)$ and the number of fissile atoms per unit of volume N_f, the volumetric heat generation rate in the reactor fuel can be expressed as [3]

$$q'''(\vec{r}) = \alpha E_R \int_0^\infty N_f \sigma_f(E) \phi(\vec{r}, E) dE \qquad (2.1)$$

where E_R is the recovered fission energy (200 Mev) and α is the part of this energy deposited in the fuel.

Substituting $\sum_f(E)$ for $N_f\sigma_f(E)$, which is the macroscopic fission cross-section of the fuel, eqn. 2. 1 can be written as,

$$q'''(\vec{r}) = \alpha E_R \int_0^\infty \sum_f(E)\phi(\vec{r},E)dE \qquad (2.2)$$

In thermal reactors most of the fission are induced by thermal neutrons. Thus $\sum_f$ is simply equal to the macroscopic fission cross-section of thermal neutrons and $\phi(\vec{r},E)$ is represented by $\phi(\vec{r})$ which is the thermal neutron flux. Therefore eqn. (2.2) becomes

$$q'''(\vec{r}) = \alpha E_R \Sigma_f \phi(\vec{r}) \qquad (2.3)$$

2.1. 5 Thermal Energy Terminologies

The thermal energy terminologies used in the Thesis are defined below [4]:

(a) Power density of the core is the thermal energy released per unit volume of the core, kW/m^3.

(b) Specific power of the fuel describes the thermal energy released per unit mass of the fuel, kW/kg or MW/ton, and

(c) Power density of the fuel also is used to describe the thermal energy released per unit volume of the fuel, MW/m^3.

2.1.6 Spatial volumetric heat generation distribution in the reactor core

Equation (2.3) shows that the distribution of heat generation rate in the reactor is determined by the distribution of the neutron flux throughout the region of the core

which contains the fuel. Since an accurate neutron flux density distribution determination is a complicated process, only cylindrical reactors with axial and radial symmetry are considered. In addition, the assumption is that the fuel elements have a constant enrichment and are uniformly distributed throughout the core. This assumption allows the treatment of the reactor core as homogeneous reactor and determines the overall features of the neutron flux distribution. However, homogeneous reactor approach can still be used to get an idea on the overall neutron flux pattern.

Using a one group neutron approach, the thermal neutron flux distribution in the core region of a homogeneous reactor with radial and axial reflectors can be approximated by:

$$\Phi = \Phi_o J_o \left(2.405 \frac{r}{R'}\right) cos \left(\pi \frac{z}{H'}\right). \quad (2.4)$$

where Φ_o is the flux at the center of the reactor, J_o is zero-order Bessel function of the first kind, r and z are the radial and axial coordinates and with reference to eqn. (2.1) vary between O and R, and 1/2H and -1/2H, respectively. R and H are the radius and the height of the reactor core and $R'$and $H'$are the effective radius and height of the core including an allowance for the reflector. R and H are respectively smaller than R' and H'.

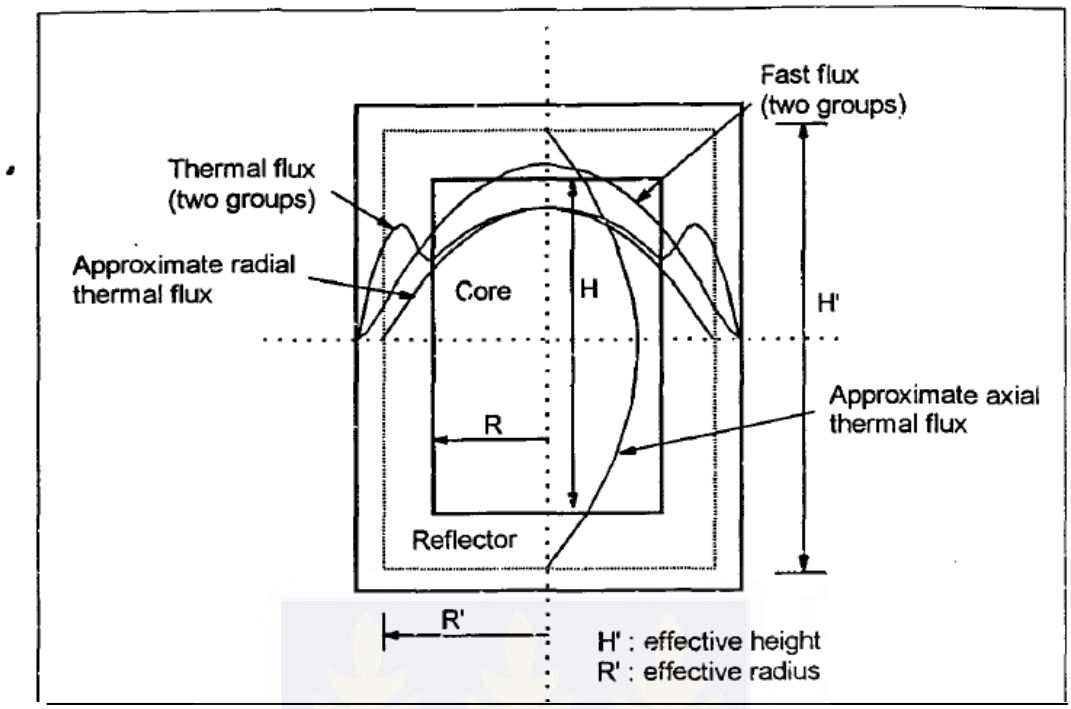

Fig 2.1 Radial and axial thermal neutron distribution obtained with eqn. (2.4) and with two neutron energy groups. [4].

The average flux in the core region is given by:

$$\bar{\phi} = \frac{1}{\pi R^2 H}\int_o^R \int_{\frac{-H}{2}}^{\frac{H}{2}} \phi 2\pi r dr dz \qquad (2.5)$$

Substituting ϕ in equation (2.4) into eqn. (2.5) and integrating yields [5]:

$$\frac{\bar{\phi}}{\phi_o} = \frac{2RR^{!}J_1\left[2.405\frac{R}{R^{!}}\right]}{2.405\,R^2}\cdot\frac{2H^{!}sin\left(\frac{\pi H}{2H^{!}}\right)}{\pi H} \qquad (2.6)$$

where J_1 is the first order Bessel function .

Equation (2.3) indicates that the heat generation rate or the power density of the core is proportional to the thermal neutron flux. For that reason equation (2.6) also gives the ratio of the heat generation rate $\frac{q'''}{q_o'''}$ where q_o''' is the maximum heat generation rate within the reactor.

In the case of bare reactor, where R= R' and H= H' the reciprocal of the ratio given by eqn. (2 .6) becomes

$$\frac{q_o'''}{q'''} = \frac{2.405}{2J_{1(2.405)}}\frac{\pi}{2} = 3.6$$

Therefore for a reactor equipped with radial and axial reflectors, it can be assumed that

$$\frac{R}{R'} = \frac{0.115}{0.138} = \frac{H}{H'} = \frac{0.23}{0.276} = 0.83$$

In this light the value of the q_o''' / q''' ratio is in the region of 2.35. For a uniform radial neutron flux, the same ratio has the value of 1.57. These simple calculations show that the maximum neutron flux or heat generation rate in the core may be substantially higher than the average neutron flux or heat generation rate.

In reactor design, a high ratio q''' / q''' is not desirable. In a given reactor, it may be possible to increase the power output by decreasing this ratio. In other words, the power output of the reactor can be increased by a more uniform distribution of the heat generation rate. This is usually referred to as flattening of the heat generation distribution or of the neutron flux [5].

2.1.7 Determination of the maximum neutron flux.

The maximum thermal neutron flux for a homogeneous reactor consisting of axial and radial reflectors is determined by using equations (2.3) and (2.4).

Using these two equations the total power of the reactor can be written as [4],

$$P_t = \int_{-1/2H}^{1/2H}\int_0^R q'''(r,z)2\pi r dr dz = \alpha E_R \hat{\Sigma}_{fm}\int_{-1/2H}^{1/2H}\int_0^R \phi_o J_o\left(2.405\frac{r}{R'}\right)\cos\pi\frac{z}{H'}2\pi r dr dz \quad (2.7)$$

where $\acute{\Sigma}_{fm}$ is the macroscopic fission cross-section of the thermal neutrons. As the reactor is homogeneous, the assumption is that all the recovered fission energy,E_R, is deposited in the core. In this case α ≈ 1.

Considering the fact that

$$\int rJ_o(\lambda r)dr = \frac{r}{\lambda}J_1(\lambda r) \tag{2.8}$$

then equation (2.7) can be integrated to obtain

$$P_t = \phi_o E_R \acute{\Sigma}_{fm} \frac{RR'}{2.405} 4H' J_1\left(2.405\frac{R}{R^!}\right) sin\frac{\pi}{2}\frac{H}{H^!} \tag{2.9}$$

Making ϕ_o the subject, eqn. (2.9) becomes

$$P_t = \phi_o E_R \acute{\Sigma}_{fm} \frac{RR^!}{2.405} 4H' J_1\left(2.405\frac{R}{R^!}\right) s \in \frac{\pi}{2}\frac{H}{H^!} \tag{2.10}$$

By making the assumption for R/R' =H/H' = 0.83, eqn. (2.10) now becomes

$$\phi_o = 2.35\frac{P_t}{E_R \acute{\Sigma}_{fm} V} \tag{2.11}$$

where V is the volume of the core.

Thus a reactor with axial and radial reflectors, we have $\frac{\phi_o}{\acute{\phi}}$ =2.35 and the total power of the reactor from eqn. (2.10) can be written as:

$$P_t = \acute{\phi}\acute{\Sigma}_{f_m} E_R V = \frac{\phi_o}{2.35}\acute{\Sigma}_{f_m} E_R V \tag{2.12}$$

Therefore, $$\phi_o = 2.35\frac{P_t}{E_R \acute{\Sigma}_{fm} V}$$

Substituting eqn. (2.11) into eqn. (2.4) the distribution of the thermal neutron flux becomes,

$$\phi = \frac{2.35 P_t}{E_R \acute{\Sigma}_{fm} V} J_o\left[2.405\frac{r}{R'}\right] cos\pi\frac{z}{H'} \tag{2.13}$$

Equation (2.13) can also be used to approximate the flux in a reactor which consists of fuel assemblies of n rods, provided that the value of $\acute{\Sigma}_{f_m}$ is computed for an equivalent homogeneous mixture.

Suppose that there are N fuel assemblies in the reactor core and each assembly consists of n rods of fuel radius r_0 and length H. Also taking $\acute{\Sigma}_{f_r}$ as the macroscopic cross-section of the fuel, the total fission cross-section of the entire core is:

$\acute{\Sigma}_{f_r} Nn\pi {r_o}^2 H$ while the average value of $\acute{\Sigma}_{f_m}$ in the core is given by:

$$\acute{\Sigma}_{f_m} = \frac{\acute{\Sigma}_{f_r} Nn\pi {r_o}^2 H}{\pi R^2 H} = \frac{\acute{\Sigma}_{f_r} Nn {r_o}^2}{R^2}. \qquad (2.14)$$

Substituting equation (2.14) into (2.13) yields;

$$\phi = 0.75 \frac{P_t}{E_R \acute{\Sigma}_{f_r} H {r_o}^2 Nn} J_o \left[2.405 \frac{r}{R'}\right] cos\pi \frac{z}{H'}. \qquad (2.15)$$

The distribution of the heat sources in the reactor is obtained by introducing equation (2.15) into eqn. (2.3) and taking $\acute{\Sigma}_f$ as being equivalent to $\acute{\Sigma}_{f_r}$; therefor

$$q'''(r,z) = \frac{0.75 \alpha P_t}{H {r_o}^2 Nn} J_o \left[2.405 \frac{r}{R'}\right] cos\pi \frac{z}{H'}. \qquad (2.16)$$

Equation (2.16) is the global distribution of the heat sources or power density in the reactor core. The dependence of q''' on the variable r gives the variation of the power density from rod assembly to rod assembly in the core but not across any individual assembly nor across the fuel rod shown in figure 2.2

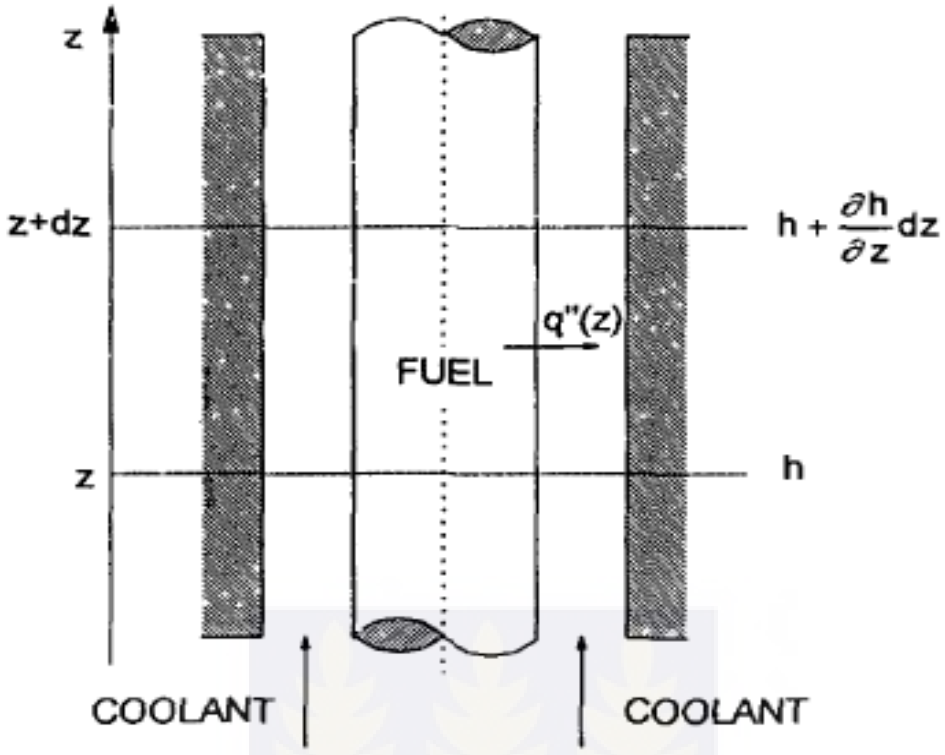

Fig 2.2 Fuel channel with single rod

Assume q''' as being constant in the fuel assembly and in the fuel rod even though this assumption is arguable for fuel assemblies any errors in the heat transfer calculations especially for small diameter natural uranium or low enrichment fuel rods used in most power reactors and MNSRs are not significant [11].

2.1.8 Maximum and Average Linear Power of the Fuel Channel

Fuel channel which consists of cylindrical fuel rods inserted in a circular cross-section channel is considered. To obtain the highest possible heat transfer from the reactor and achieving the maximum fuel temperature below the permissible value, the heat transfer should be increased. For each fuel rod, the heat transfer surface may be increased either by dividing it into a number of small diameter rods or by adding fins on the cladding of the rod.

Considering the neutron flux distribution given by equation (2.16), that the maximum power density is at the center of the core where r=0 and z =0, and both functions in eqn. (2.16) are unity and the maximum value is;

$$q'''_{max} = \frac{0.75\alpha P_t}{H r_o^2 Nn}.$$

Hence the power density distribution throughout the reactor can be stated as;

$$q''' = q'''_{max} J_o\left[2.405\frac{r}{R'}\right]cos\pi\frac{z}{H'} \qquad (2.17)$$

From equation (2.17), the power density distribution in a fuel channel located at a given radial distance is given by;

$$q''' = q_o'''cos\pi\frac{z}{H'} \qquad (2.18)$$

where $q_o''' = q'''_{max} J_o\left[2.405\frac{r}{H'}\right]$. Equation (2.18) can be expressed conveniently as:

$$q''' = q_o'''cos2\pi\frac{H}{2H'}\frac{z}{H} = q_o'''cos2\pi\beta\frac{z}{H} \qquad (2.19)$$

Using equation (2.19) the average power density in a fuel channel can be written as:

$$q'''_{av} = \frac{\int_{-½H}^{½H} q_o''' cos2\pi\beta\frac{z}{H}dz}{\int_{-½H}^{½H} dz} = q_o'''\frac{sin\beta}{\beta} \qquad (2.20)$$

The liner power distribution along the channel is obtained by multiplying equation (2.20) by the cross sectional area of the fuel;

$$q' = n\pi r_o^2 q_o'''cos2\beta\frac{z}{H} = q'_o cos2\beta\frac{z}{H} \qquad (2.21)$$

where n is the number of the rods in the fuel assembly. By integrating eqn. (2.21) along the channel gives the total fuel channel power as;

$$P_c = \int_{-½H}^{½H} n\pi r_o^2 q_o'''cos2\beta\frac{z}{H}dz = \int_{-½H}^{½H} q'_o cos2\beta\frac{z}{H}dz = q_o' H\frac{sin\beta}{\beta} \qquad (2.22)$$

By taking $q'_{av} = q_o'\frac{sin\beta}{\beta}$ (2.23)

Equation (2.22) then becomes

$$P_c = H q'_{av} \qquad (2.24)$$

2.2 Thermal-hydraulics of a fuel channel

The thermal-hydraulics equations consist of the energy conservation equations applied to the coolant, the cladding and to the fuel with appropriate boundary conditions. To determine the coolant energy conservation equation, a single fuel channel is considered as shown in Fig. 2.2 with control volume laterally limited by the channel wall and the fuel, and axially by the planes z and z+ dz. The analysis on a single fuel rod can be easily extended to a multi-rod fuel bundle provided that a strong mixing exists between the laterally interconnected sub-channels bounded by the fuel rods or by the fuel rods and the channel wall.

The application of energy conservation principle to the chosen control volume gives equation of the form,

$$\left(h+\frac{\partial h}{\partial z}dz\right)GAd\tau+\frac{\partial u}{\partial \tau}Adzpd\tau=hGAd\tau+q_c{}''sdzd\tau \tag{2.25}$$

or $$\rho\frac{\partial u}{\partial \tau}+G\frac{\partial h}{\partial z}=\frac{q_c{}''}{A}s \tag{2.26}$$

for energy and mass conservation where

$q_c{}''$ is heat on the fuel element surface, kW/m^2 ^oC,

A is channel flow area (m^2),

s is heated perimeter (m),

ρ is fluid specific mass (kg/m^2),

u is specific internal energy (kJ/kg),

h is specific enthalpy (kJ/kg),

τ is time (s).

Assuming that the heat conduction in the axial and angular directions are negligible compared to that in the radial direction, the following conduction equations holds for the fuel element [6].

$$\frac{1}{r}\frac{\partial}{\partial r}\left(k_f r\frac{\partial T}{\partial r}\right)+q'''=\frac{\partial}{\partial \tau}\left(\rho_f c_f T\right) \qquad r\le r\le r_o \tag{2.27}$$

and for the cladding:

$$\frac{1}{r}k_c\frac{\partial}{\partial r}\left(r\frac{\partial T}{\partial r}\right)=\frac{\partial}{\partial \tau}\left(\rho_c c_c T\right) \qquad r_o\le r\le r_c \tag{2.28}$$

where:

k_f is conductivity of the fuel, usually a strong function of the temperature, W/m^oC.

k_c *is* conductivity of the cladding, it may be taken as constant (W/m^oC)

ρ *is* specific mass (f-fuel, c-cladding) (kg/m^2)

c is specific heat (J/kg)

q''' is power density (W/m^2)

The control variables and boundary conditions for eqns. (2.27) and (2.28) are:

1. Inlet mass flow rate (kg/s)
2. Inlet temperature (°C)
3. Inlet pressure (Pa or MPa)
4. Heat convection at the fuel element surface:

$$-k_c\left(\frac{\partial T_c}{\partial r}\right)h_c(T_c(r_c)-T) \qquad r=r_c \tag{2.29}$$

where

h_c is convective heat transfer ($W/m^2\ ^oC$),

$T_c(r_c)$ is the temperature on outer surface of cladding (°C),

T is temperature of the coolant (°C),

r_c is radius of the fuel element (m).

5. Heat transfer at the fuel-cladding interface:

$$q'' = h_g (T_f (r_o) - T_c (r_o) \quad (2.30)$$

where:

h_g gap conductance, W/m^2 °C,

$T(r_o)$ temperature at the surface of the fuel, °C

$T_c(r_o)$ temperature at the inner surface of the cladding, °C

6. Continuity of the heat fluxes at the fuel-cladding interface:

$$k_f \left(\frac{\partial T_f}{\partial r}\right) = k_c \left(\frac{\partial T_c}{\partial r}\right), \qquad r = r_o. \quad (2.31)$$

2.3. Gap conductance between the fuel and cladding.

In manufacturing the fuel rods, a gap of about 0.08 mm is created between the outer surface of the fuel and the inner surface of the cladding in order to insert easily the fuel pellets into the cladding tubes. In some reactors graphite powder is used to facilitate the insertion of fuel pellets. The cladding tubes are filled at atmospheric pressure with an inlet gas such as helium to avoid corrosion and assure a reasonable initial heat transfer [20]. Since the gap is so small, the convection currents cannot develop in the gas. The heat transfer in the gap region is by conduction through the filling gas. Because of the swelling and the thermal expansion of the fuel, the gap region closes and the direct contact between the surfaces at several discrete points take place. Consequently, the heat transfer by conduction at these points should be taken into account when modeling the heat transfer through the gap region [7].

The gap heat transfer are usually expressed in terms of a gap heat transfer coefficient or conductance, h_g. Taking the temperature on the fuel surface and on the inner

surface of the cladding as T_f and T_c' respectively, then the linear heat flux across the gap is:

$$q' = 2\pi r_o h_g (T_f - T_c'). \quad (2.32)$$

The gap heat transfer coefficient (gap conductance) has been considered for two general cases of open and closed gaps [8].

2.3.1 Open gap.

If the fuel and cladding is not in physical contact, which is true for fresh fuel or fuel operating at very low linear power rate, the fuel stands freely within the cladding. In this case the heat transfer mechanisms are conduction through the filling gas and radiation.

If the space between the fuel and the cladding is larger than the mean free path of the atoms at the prevailing temperature and pressure, the gap conductance, considering also the heat exchange by radiation between the exposed surfaces, is given by [9]

$$h_g = \frac{k_g}{\delta_g} + \frac{\sigma}{\frac{1}{\varepsilon_f}+\frac{1}{\varepsilon_c}-1}\frac{T_f^4 - T_c^{!4}}{T_f - T_c} \quad (2.33)$$

where k_g is the thermal conductivity of the gas, δ_g is the gap thickness, σ is the Stefan-Boltzman constant, ε_f and δ_c are the surface emissivities of the fuel and cladding respectively. In cases of small gaps where the temperature gradient is also sustained, a steep change in the gas temperature is observed in the region close to the solid surfaces. The variation of the gas temperature in the gap region is a steep change that takes place within a mean free path from the walls and is called the temperature jump denoted by distances δ_f and δ_c in figure (2.4) [10].

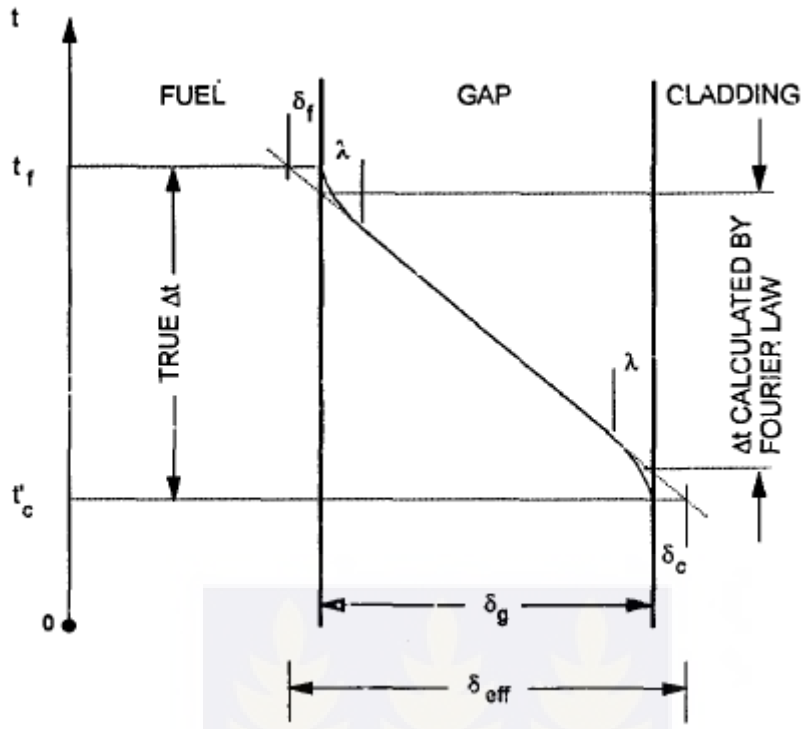

Fig 2.3 Temperature profile in the region and temperature jump [10].

The extrapolation of the temperature profile in the bulk of the gas intersects the fuel and cladding temperature in the solids at distances δ_f and δ_c respectively. These distances are called temperature jump distances and should be added to the actual gap thickness in order to predict the correct fuel –cladding temperature difference by using the Fourier conduction law. The conductance for narrow gaps of few mean free path is then given by [9]

$$h_g = \frac{k_g}{\delta_g+\delta_f+\delta_c} + \frac{\sigma}{\frac{1}{\varepsilon_f}+\frac{1}{\varepsilon_c}-1}\frac{T_f{}^4-T_c{}'^4}{T_f-T_c{}'} \tag{2.34}$$

Kennard [10] gives the temperature jump distance as:

$$\delta = 2\left(\frac{2-\alpha}{\alpha}\right)\left(\frac{r}{1-r}\right)\left(\frac{k}{\mu c_p}\right)\boldsymbol{\lambda}. \tag{2.35}$$

where **λ** is mean free path in the gas, r is the radial distance change and is the ratio of $\frac{c_p}{c_v}$ for the gas, c_p is specific heat at constant pressure, μ is velocity of the gas and k

the conductivity of the gas. α is the thermal accommodation coefficient of the gas in contact with a solid surface,

$$\alpha = \frac{T_r - T_i}{T_s - T_i} \tag{2.36}$$

T_i is the temperature of molecules that strike the solid, T_s is the temperature of the solid and T_r is the temperature of the reflected molecules. The mean free path is given by:

$$\lambda = \frac{\lambda_o}{p}\frac{T}{273} \tag{2. 37}$$

where T is the absolute temperature in Kelvin, p is gas pressure in bar and λ_o is the property of the gas that depends on the molecular or atomic diameter [10]

2.3.2. Closed gap.

In practice, because of the fuel swelling, the differential expansion of the fuel and the pressure exerted by the coolant on the outside surface of the cladding, the gap tends to close. As a result the gap reduces and because of the roughness of the fuel and cladding surfaces, solid-to-solid contact between them will be established. Under this condition, heat transfer in the gap region occurs through the points of solid contact and across the discontinuous gas gap between these points of contact. Figure (2.4) shows how the closed gap may look like.

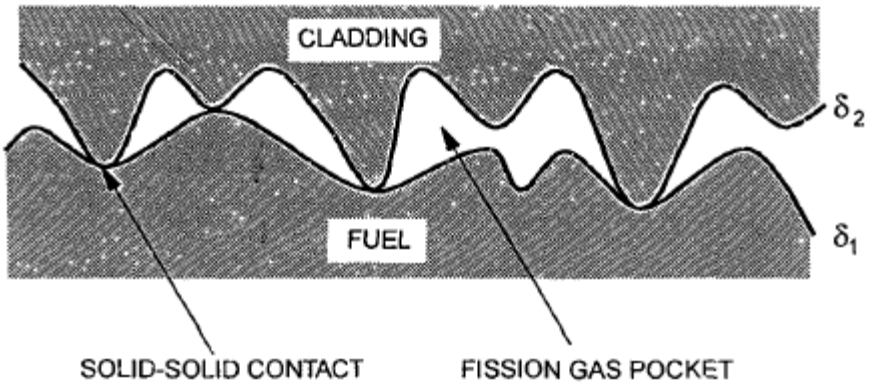

Fig. 2.4. Closed fuel-cladding gap.

The different components of conductance in a closed gap are [20]

(a). Gas conductance through discontinuous gap, h_g.

(b). Conduction through the solid-to-solid contact points , h_s.

(c). Radiation through the discontinuous gap, h_r

According to the work of Cetinkale and Fisherden [8] the following relationship for the conductance due to solid-to-solid contact is established.

$$h_s = A\frac{2k_f k_c}{k_f + k_c}\frac{P_i}{H\delta^{½}} \qquad (2.38)$$

where

A dimensional constant, $m^{½}$ (=$10m^{½}$).

k_f conductivity of the fuel,$W/m^o\ C$.

k_c conductivity of the cladding, $W/m^o\ C$

P_i surface contact pressure, N/m^2.

H Meyer hardness number of softer material N/m^2.

δ root- mean-squre of contact material surface rughness and is given by:

$[\frac{\delta_1^2 + \delta_2^2}{2}]^{½}$ m

where δ_1, δ_2 are the surface roughness of the interface material, m.

Ross and Stoute [6] assumed that the thickness of a closed gap is related to the surface roughness as:

$$\delta_g = C(\delta_1 + \delta_2) \tag{2.39}$$

Where C is a constant which depends on the interface pressure. The proposed correction for this constant is:

$$C = 2.75 - 2.55X10^{-8}\, P_i \tag{2.40}$$

where P_i is the pressure at the interface in N/m^2.

Substituting eqn. (2.39) into eqn. (2.34) and neglecting the radiation term yields;

$$h_g = \frac{k_g}{C(\delta_1+\delta_2)+\delta_f+\delta_c} \tag{2.41}$$

The total conductance, h_{con} of a closed gap is obtained by adding eqns. (2.38) and (2.41) and considering heat exchanges by radiation between the fuel and cladding:

$$h_{con} = A\frac{2k_fk_c}{k_f+k_c}\frac{P_i}{H\delta^{½}} + \frac{k_g}{C(\delta_1+\delta_2)+\delta_f+\delta_c} + \frac{\sigma}{\frac{1}{\varepsilon_f}+\frac{1}{\varepsilon_c}-1}\frac{T_f^4-T_c'^4}{T_f-T_c'} \tag{2.42}$$

2.4. LabVIEW Simulation

The cornerstone of modern engineering studies and practices is the investigation of the engineering system process by simulation. LabVIEW was used to simulate the temperature distribution in the reactor fuel-channel elements based on analytical mathematical models derived from the generation of heat in nuclear reactor fuel.

2.4.1. General Procedure

From the front panel window, a numeric control button was created to input the power to generate the axial temperature profile.

The control was linked directly in the block diagram to provide the necessary data for computation of the temperature values.

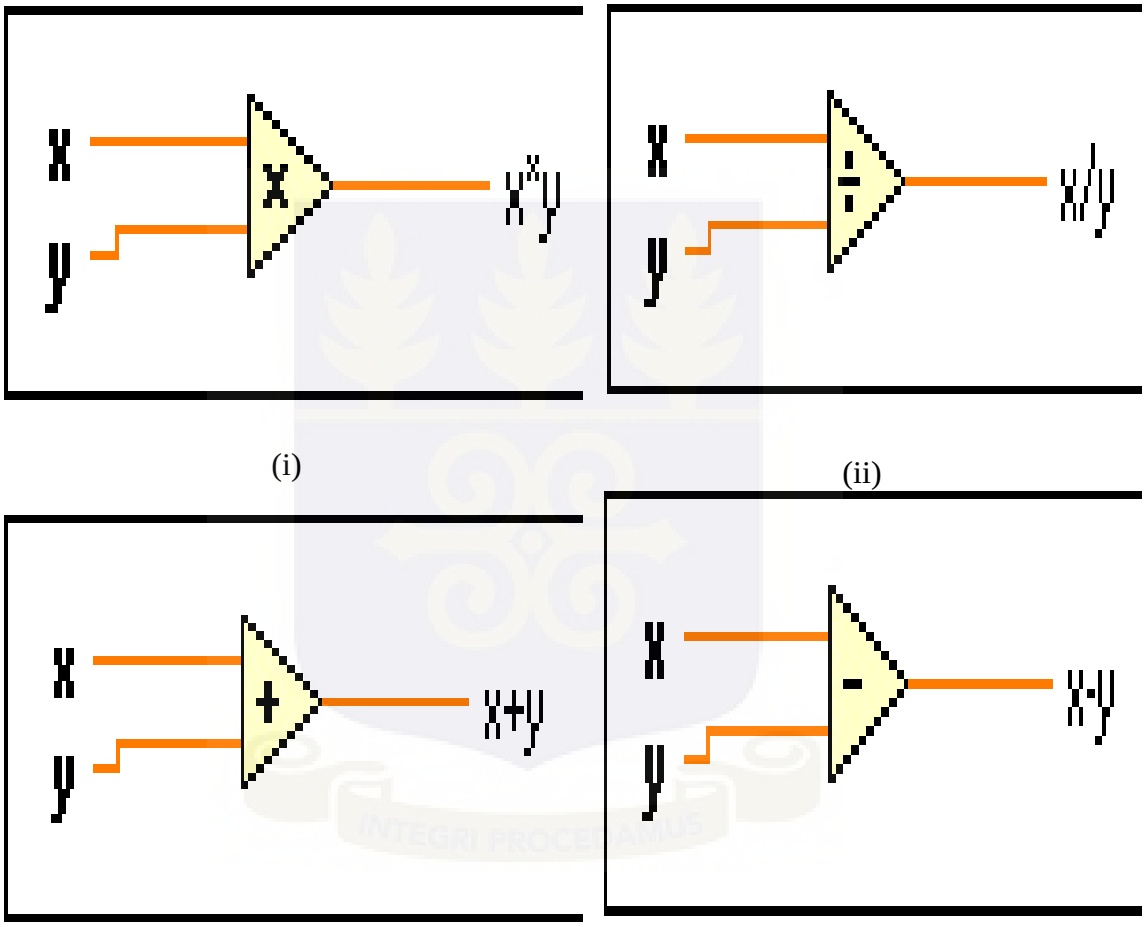

Fig 2.5 Four basic arithmetic operator functions used in the LabVIEW simulation

Figure 2.5 shows the four basic arithmetic operator functions that were used in developing the governing relations. These functions accepted only two varying data types and produced a single output. Figures 2.5 (i), (ii), (iii) and (iv) represents the multiplication, division, addition and subtraction functions respectively.

2.4.2. For Loop Programming Structure

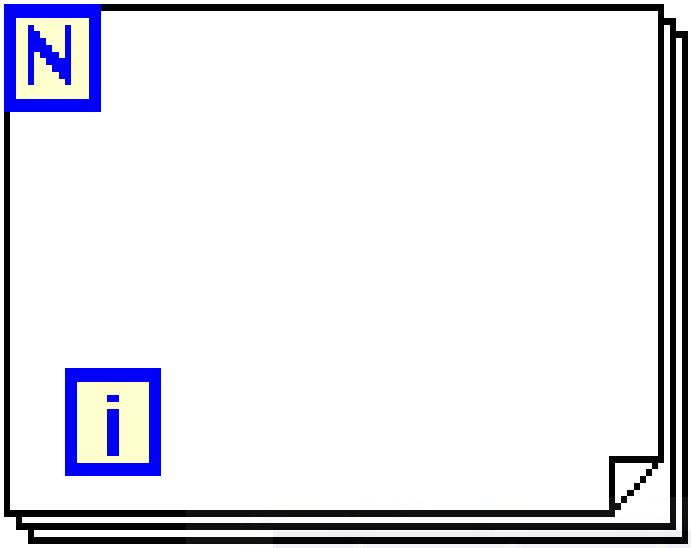

Fig 2.6 The For Loop programming structure in LabVIEW

Figure 2.6 shows the For loop programming structure used to generate the range of values representing the distance along the fuel element. The structure executed a sub-diagram n times, where n is the value wired to the count (N) terminal. The iteration (i) terminal produced the current loop iteration count which ranges from 0 to n-1. For the simulation, an axial length of 0.23 m of fuel element was divided into two where the ranges -0.115 m to 0.0 m represented the lower half and 0.0 m to 0.115 m the upper half.

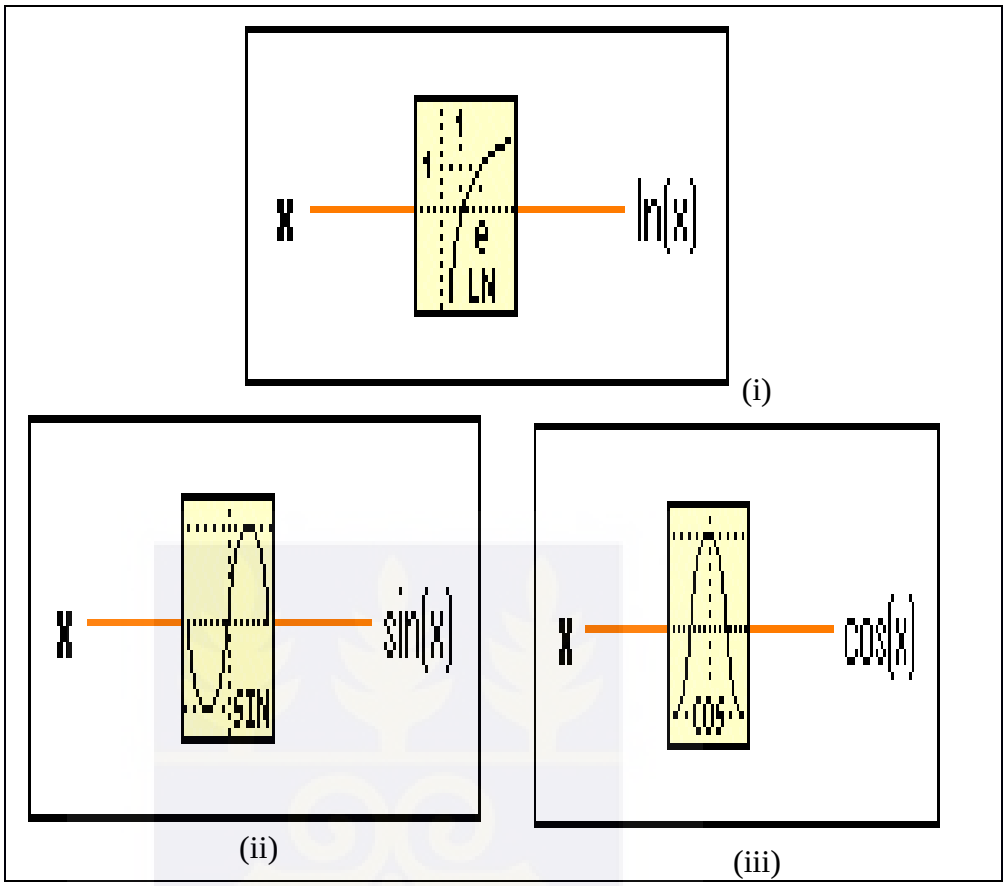

Fig 2.7 Mathematical functions in LabVIEW

The LabVIEW functions for sine, cosine and natural logarithm were also employed and functions accepted only one input to produce a single output. The input for the functions was either a 1-D array of values or a single data type value.

Figure 2.7 (i), (ii) and (iii) represent the sine, cosine and natural logarithmic functions used in Lab VIEW.

CHAPTER THREE

RESEARCH METHODOLOGY

3.1. Overview

There has been limited research work carried out on computer simulation of the temperature distribution in the MNSR reactor core. Numerical experimentation work was conducted to model and simulate the governing equations which relate to temperature distribution in the components of the reactor core by LabVIEW in order to improve on the existing knowledge and to advance the understanding of behavior of the reactor core due to temperature changes (steady state and transient, etc).

3.2 Analytical equations of temperature distribution in the reactor core components

Four analytical equations of the temperature distribution in the coolant, outer surface of the cladding, fuel surface and fuel center in the axial direction and three in the coolant, cladding and fuel in the radial direction were derived for simulation.

3.2.1. Coolant temperature along the fuel channel in axial direction.

Assuming steady state conditions, equation (2.26) can be expressed as:

$$GA\frac{dh}{dz}q_c''s \qquad (.3.1)$$

or

$$\acute{m}\frac{dh}{dz} = q' \qquad (3.2).$$

where $\acute{m}$ is the mass flow rate and q' is the linear heat flux or power density whose variation along the channel is given by eqn. (2.21). Substituting q' in eqn. (3.2) into

eqn. (2.21) and integrating the resulting equation between the inlet of the channel located at z = -½H and a given location z, illustrated by Fig. (3.1), gives;

$$\acute{m}\int_{h_i}^{h} dh = \int_{-½H}^{z} q_o{}' cos2\beta \frac{z}{H} dz \tag{3.3}$$

or $$h = h_i + \frac{q_o{}'}{\acute{m}} \frac{H}{2\beta} sin\beta \left[\frac{sin2\beta \frac{z}{H}}{sin\beta} + 1\right] \tag{3.4}$$

By substituting $q_o{}'$ in equation (2.22) into equation (3.2) yields:

$$h = h_i + \frac{P_c}{2\acute{m}} \left[\frac{sin2\beta \frac{z}{H}}{sin\beta} + 1\right]. \tag{3.5}$$

Taking $(h - h_i) \approx \acute{c}_{p(T-T_i)}$, equation (3.5) can be expressed in the temperature form as:

$$T = T_i + \frac{P_c}{2\acute{m}\acute{c}_p} \left[\frac{sin2\beta \frac{z}{H}}{sin\beta} + 1\right] \tag{3.6}$$

or recalling that the total channel power is given by:

$$P_c = \acute{m}(h_e - h_i) = \acute{m}\acute{c}_p(T_e - T_i) \tag{3.7}$$

The coolant temperature can be expressed as:

$$T = \frac{T_i - T_e}{2} + \frac{T_e - T_i}{2sin\beta} sin2\beta \frac{z}{H} \tag{3.8}$$

where h_e and T_e are the coolant enthalpy and temperature at the channel exit respectively.

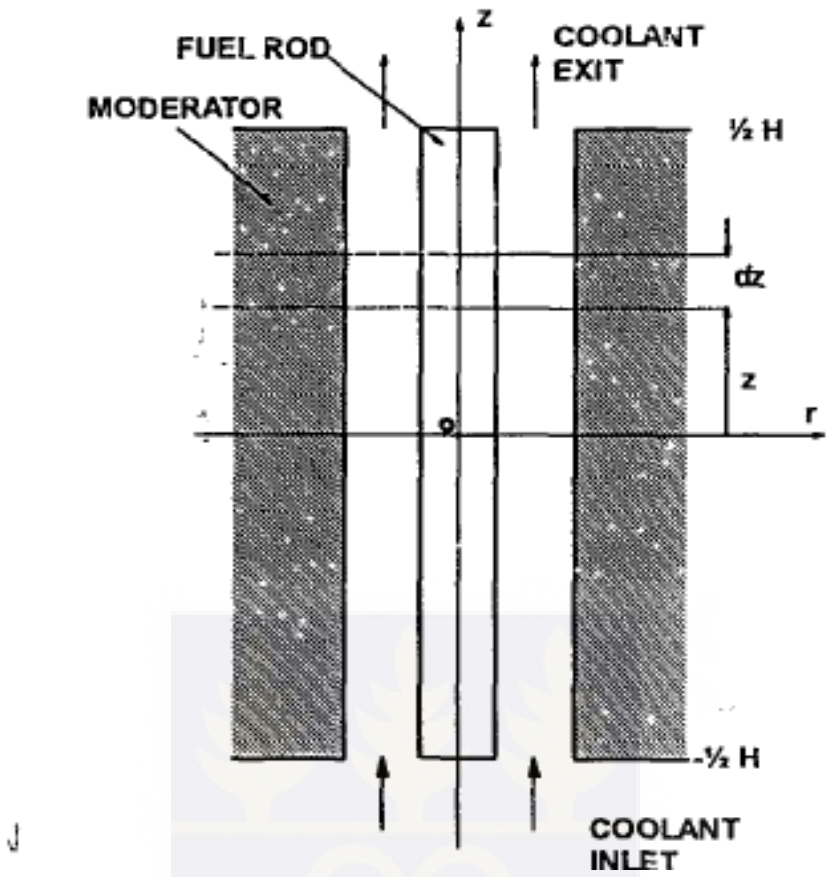

Fig. 3.1 Fuel channel

3.2.2. Temperature of the cladding.

The temperature of the outside surface of the cladding is obtained by using Newton cooling law [6]:

$$T_c - T = \frac{q'}{h_c s} \tag{3.9}$$

where T is the outside temperature of the cladding, h_c is the transfer coefficient and s is the heated perimeter. Substituting eqns. (3.8) and (2.21) into eqn. (3.9) and taking into account eqns. (2.23) and (2.24) yields :

$$T_c = \frac{T_i + T_e}{2} + \frac{T_e - T_I}{2\sin\beta} \sin 2\beta \frac{z}{H} + \frac{1}{h_c s} \frac{P_c}{H} \frac{\beta}{\sin\beta} \cos 2\beta \frac{z}{H} \tag{3.10}$$

or $$T_c = \frac{T_i + T_e}{2} + \frac{T_e - T_i}{2\sin\beta} \left(\sin 2\beta \frac{Z}{H} + \frac{1}{\gamma} \cos 2\beta \frac{z}{H}\right) \tag{3.11}$$

where $\gamma = \frac{h_c sH}{2\beta \acute{m} \acute{c}_p}$ (3.12)

by substituting for P_C the expression $\acute{m}\acute{c}_p(T_e - T_i)$ obtained in eqn. (3.7).

Taking derivative of equation (3.11), equating to zero and solving yields:

$$\frac{dT_c}{dz} = cos2\beta \frac{z}{H} - \frac{1}{\gamma} sin\beta \frac{z}{H} = 0 \quad (3.13)$$

$$\gamma = tan2\beta \frac{z}{H}$$

It follows that the maximum temperature is then located at:

$$z_m = \frac{H}{2\beta} \arctan(\gamma)$$

with the value of $T_c\ max = \frac{T_i + T_e}{2} + \frac{T_e - T_i}{2sin\beta}$ [sin (arctanγ) + $\frac{1}{\gamma}$ cos (arctan γ)] (3.14)

The maximum cladding temperature should be less than the maximum allowable temperature with a reasonable safety margin. As an example, the maximum allowable temperature for Zircaloy-4 cladding ranges from $380°C - 400°C$ [6].

The temperature distribution in the cladding in the radial direction at a given axial location is determined by using eqn. (2.28). Considering steady state condition, this equation becomes $\frac{1}{r} k_c \frac{d}{dr}\left(r \frac{dT}{dr}\right) = 0$ with $r_o \leq r \leq r_c$. (3.15)

where heat conduction in the angular and axial directions are neglected compared to that in the radial direction. Integrating eqn. (3.15) yields;

$$T_c = Alnr + B \quad (3.16)$$

To determine the constants A and B, take the inner surface of the cladding subject to a constant linear heat flux, q' whereas the outer surface is kept at the temperature T_c thus the boundary conditions can be expressed as:

$$r = r_o \qquad q' = -2\pi r_o k_c \frac{dT}{dr}$$

$$r = r_c \qquad T = T_C$$

The constants A and B are evaluated as

$$A = \frac{q'}{2\pi k_c} \tag{3.17}$$

$$B = T_c + \frac{q'}{2\pi k_c} ln r_c \tag{3.18}$$

Therefore the variation of the temperature through the cladding is given by:

$$T = T_c + \frac{q'}{2\pi k_c} ln \frac{r_c}{r} \text{ with } \quad r_o \leq r \leq r_c. \tag{3.19}$$

Finally, the inner surface temperature of the cladding is obtained by setting $r = r_o$:

$$T_c' = T_c + \frac{q'}{2\pi k_c} ln \frac{r_c}{r_o} \tag{3.20}$$

3.2.3. Temperature profile of fuel element

Combining eqns. (3.20) and (2.32), an expression for the surface temperature of the fuel is obtained as;

$$T_f = T_c + \frac{q'}{2\pi k_c} ln \frac{r_c}{r_o} + \frac{q'}{2\pi r_o h_{con}} \tag{3.21}$$

The variation of T_c is given by eqn. (3.11). Replacing this equation into the above equation and taking into consideration equations (2.21) and (2.22) we obtain :

$$T_f = \frac{T_i + T_g}{2} + \frac{T_g - T_i}{2sin\beta} [sin\beta\frac{z}{H} + (\frac{1}{\gamma} + \frac{\beta}{2\pi k_c} \frac{P_C}{(T_g - T_i)H} \text{ In } \frac{r_c}{r_o} + \frac{\beta}{\pi r_o h_{con}} \frac{P_C}{(T_g - T_i)H}) cos2\beta\frac{z}{H} \tag{3.22}$$

By letting $\frac{1}{\gamma'} = \frac{1}{\gamma} + \frac{\beta}{2\pi k_c} \frac{P_C}{(T_g - T_i)H} \text{ In } \frac{r_c}{r_o} + \frac{\beta}{\pi r_o h_{con}} \frac{P_C}{(T_g - T_i)H})$ (3.23)

Equation (3.22) can be expressed as:

$$T_f = \frac{T_i + T_g}{2} + \frac{T_g - T_i}{2sin\beta} \left[sin2\beta \frac{z}{H} + \frac{1}{\gamma'} cos2\beta \frac{z}{H} \right] \tag{3.24}$$

Differentiating equation (3.24) with respect to z to obtain the location of the maximum temperature as:

$$\frac{\partial T_f}{\partial z} = cos2\beta \frac{z}{H} - \frac{1}{\gamma'} sin2\beta \frac{z}{H} = 0 \tag{3.25}$$

$$z_m = \frac{H}{2\beta} arctan\gamma' \tag{3.26}$$

Therefore maximum temperature is:

$$\boldsymbol{T_{fmax}} = \frac{T_i+T_e}{2} + \frac{T_e-T_i}{2sin\beta}\left[sin(arctan\gamma') + \frac{1}{\gamma'} cos(arctan\gamma')\right] \tag{3.27}$$

3.2.4. Temperature profile in the fuel center

To determine the temperature distribution in the fuel and analyze the variation of fuel centerline temperature along the channel, the following assumptions were made:

(a) The neutron flux within the fuel pellet and heat generation rate are uniform.

(b) No angular variation in convective heat transfer coefficient and in the gap conductance no significant angular temperature gradient exists in the fuel.

(c) The axial conduction of heat is small compared to that in radial direction which is confirmed by length to diameter ratio being higher than 20.

(d) The steady state conditions prevail, [11, 21].

Based on the above conditions equation (2.27) can be written as :

$$\frac{1}{r}\left(\frac{d}{dr} k_f r \frac{dt}{dr}\right) + q'' = 0 \tag{3.28}$$

Integrating equation (3.28) gives;

$$k_f r \frac{dT}{dr} + q''' \frac{r^2}{2} + A = 0 \leftrightarrow k_f \frac{dT}{dr} q''' \frac{r}{2} + \frac{A}{r} = 0 \tag{3.29}$$

Assuming that the fuel has an internal cavity of radius $r_i$which is not cooled and there is no heat flux at r_i, a corresponding boundary condition is written as:

$$q''_{r=r_o} = -k_f \frac{dT}{dr}\Big|_{r=r_i} = 0 \quad (3.30)$$

Therefore the constant A can be determined: $A = \frac{q'''r_i^2}{2}$ (3.31)

Integrating eqn. (3.29) from r to r_o which is outside the fuel diameter gives:

$$\int_T^T k_f\, dT = \frac{-q'''}{4}(r_o^2 - r^2) + \frac{q'''}{2} r_i^2 ln\frac{r_o}{r} \leftrightarrow \int_{T_f}^T k_f\, dT = \frac{q'''r_o^2}{4}[1 - \left(\frac{r}{r_o}\right)^2 -$$

$(\frac{r_i}{r_o})^2$ In$(\frac{r_o}{r})^2]$ (3.32)

In the case of a fuel pellet where r_i = 0 the eqn. (3.32) becomes;

$$\int_{T_f}^T k_f\, dT = \frac{q'''r_o^2}{4}\left[1 - \left(\frac{r}{r_o}\right)^2\right] \quad (3.33)$$

A relationship between the temperature at the center T_o, at the surface T_f and the radius of the fuel can be obtained by substituting in eqn. (3.33) r =0;

$$\int_{T_f}^T k_f dT = \frac{q'''r_o^2}{4} \quad (3.34)$$

Equation (3.34) is equivalent to $\int_T^{T_o} k_f dT = \frac{q'}{4\pi}$ (3.35)

where q' is the linear power or heat flux which is given by $q' = \pi r_o^2 q'''$.

For a constant conductivity equation (3.33) can be integrated to obtain the radial temperature distribution in the fuel;

$$T = T_f + \frac{q'}{4\pi k_f}[1 - \left(\frac{r}{r_o}\right)^2] \quad (3.36)$$

The fuel center temperature of the fuel is obtained by putting r=0;

$$T_o = T + \frac{q'}{4\pi k_f} \quad (3.37)$$

Using equations (2.21), (2.23), (2.24) and (3.24) the variation of the fuel center temperature along the channel is obtained:

$$T_o = \frac{T_i+T_e}{2} + \frac{T_e-T_i}{2sin\beta}\left[sin\beta\frac{z}{H} + \frac{1}{\gamma''}cos2\beta\frac{z}{H}\right] \quad (3.38)$$

where

$$\frac{1}{\gamma''} = \frac{1}{\gamma'} + \frac{\beta}{2\pi k_f}\frac{P_C}{(T_e-T_i)H} \quad (3.39)$$

The maximum centerline temperature is located at:

$$z_{max} = \frac{H}{2\beta}arctan\gamma'' \quad (3.40)$$

and the maximum value is:

$$T_{omax} = \frac{T_i+T_e}{2sin\beta} + \frac{T_e-T_i}{2sin\beta}\sqrt{1+\left(\frac{1}{\gamma''}\right)^2} \quad (3.41)$$

3.3. Temperature profile in the radial direction.

The appropriate steady-state heat transfer relations needed in determining the radial temperature profile of nuclear reactor channel involves conservation of energy in a cylindrical differential volume element in the fuel :

$$q'''(r,z) = \underset{\rightarrow}{\Delta}\ \underset{\rightarrow}{q''}(r,z) \quad (3.42)$$

and the Fourier's law of heat conduction

$$\underset{\rightarrow}{q''}(r,z) = -k\ \underset{\rightarrow}{\Delta}\ T(r,z) \quad (3.43)$$

where

T(r, z) – local medium temperature °C

k – thermal conductivity of the medium, W/m^2

$\underset{\rightarrow}{q''}(r,z)$– vector heat flux, W/$m^2$

$q'''(r,z)$ – power density, W/m^3.

The power density is zero everywhere except in the nuclear fuel region. In the fuel region it is defined in terms of the fission process:

$$q'''(r,z) = \gamma\int_0^\infty \Sigma_f(r,z,E)\varphi(r,z.E)dE \quad (3.44)$$

Figure 2.6 illustrates the material composition of the fuel rod, viz fuel, sheath-cladding, coolant cell. The thermal conductivities in each material have been determined. We indicate the local temperature at specific radial coordinates [12].

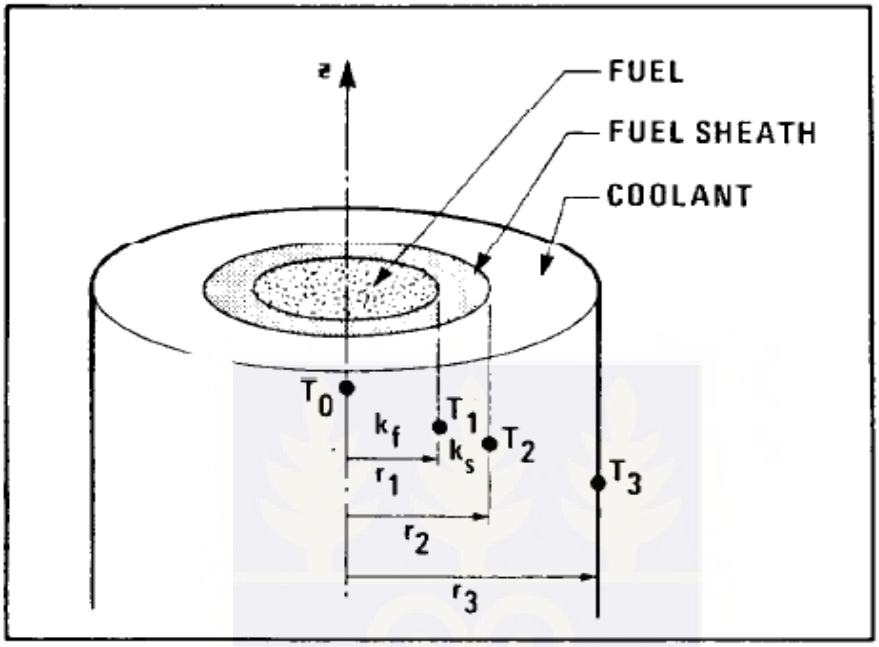

Fig. 3.2. Definition sketch that is used in the determination of radial temperature profile in a fuel – sheath –coolant of nuclear reactor channel.

3.3.1. Fuel temperature profile in the radial direction

Using equations (3.42) and (3.43) yields;

$$q'''(r,z) = \underset{\rightarrow}{\nabla}.\underset{\rightarrow}{q}''(r,z) = \underset{\rightarrow}{\nabla}.\left[-k_f \underset{\rightarrow}{\nabla} T_f(r,z)\right] \qquad (3.45)$$

Restricting the analysis to a specific z-coordinate and taking the thermal conductivity,k_f, and nuclear power density, q''', as constants permits the integration of eqn. (3.45) twice to obtain the radial fuel temperature, $T_{f(r)}$ in terms of two constants of integration. These constants are determined by imposing the conditions that $T_{f(r)}$ is finite in the fuel and equal to T_a , temperature at the fuel sheath interface [20].

Thus $T_{f(r)} = T_a + \frac{q'''}{4k_f}(r_1{}^2 - r^2)$ (3.46)

a quadratic function in r.

3.3.2. The temperature profile of the cladding in the radial direction.

The heat flux in the radial direction is, however, linear in r;

$$q_f{}''(r) = -k_f \frac{dT_{f(f)}}{dr} q''' \frac{r}{2} \quad (3.47)$$

Since no energy is generated in the sheath, q''' is zero in the sheath and we write eqn. (3.42) as:

$$\underset{\rightarrow}{\Delta}.\underset{\rightarrow}{q}''(r) = 0 \quad (3.48)$$

and finally obtain $T_d(r)$ temperature profile in the sheath:

$$T_d(r) = T_a - \frac{r_1 q_s{}''(r_1)}{k_s} ln\left(\frac{r}{r_1}\right). \quad (3.49)$$

3.3.3. The temperature profile of the coolant in the radial direction

The mean temperature in the coolant, $T_{h(r)}$, may be represented with the aid of Newton's law of cooling by

$$q''(r_2) = h(T_b - T_h) \quad (3.50)$$

where h is the film coefficient of heat transfer. Therefore, we write

$$T_{h(r)} = T_b - \frac{q''(r_2)}{h} = T_b - \frac{q'''}{2hr_2} r^2 \quad (3.51)$$

3.4 Summary of equations of the temperature distribution for simulation and visualization

3.4.1 Analytical equations of temperature distribution in the axial direction adopted for the simulation and visualization

1. Coolant: $T = \frac{T-T_e}{2} + \frac{T_e - T_i}{2sin\beta} sin2\beta \frac{z}{H}$

2. Outer surface of the cladding:

$$T_c = \frac{T_i+T_e}{2} + \frac{T_e-T_i}{2sin\beta} sin2\beta \frac{z}{H} + \frac{1}{h_c s} \frac{P_c}{H} \frac{\beta}{sin\beta} cos2\beta \frac{z}{H}$$

we can call the underlined expression: $\gamma = \frac{h_c sH}{2\beta \acute{m} \acute{c}_p}$

3. Fuel surface:

$$T_f = \frac{T_i+T_e}{2} + \frac{T_e-T_i}{2sin\beta} [\sin\beta\frac{z}{H} + (\frac{1}{\gamma} + \frac{\beta}{2\pi k_c} \frac{P_C}{(T_e-T_i)H} \text{In} \frac{r_c}{r_o} + \frac{\beta}{\pi r_o h_{con}} \frac{P_C}{(T_e-T_i)H}) \cos2\beta\frac{z}{H}$$

alternatively $\frac{1}{\gamma} + \frac{\beta}{2\pi k_c} \frac{P_C}{(T_e-T_i)H} \text{In} \frac{r_c}{r_o} + \frac{\beta}{\pi r_o h_{con}} \frac{P_C}{(T_e-T_i)H}) = \frac{1}{\gamma'}$

4. Fuel center: $T_o = \frac{T_i+T_e}{2} + \frac{T_e-T_i}{2sin\beta} [sin2\beta \frac{z}{H} + \frac{1}{\gamma''} cos2\beta \frac{z}{H}]$

where $\frac{1}{\gamma''} = \frac{1}{\gamma'} + \frac{\beta}{2\pi k_f} \frac{P_C}{(T_e-T_i)H}$

3.4.2 Analytical equations of temperature distribution in the radial direction adopted for the simulation and visualization

5. Fuel: $T_f = T_a + \frac{q'''}{4k_f}(r_1{}^2 - r^2)$

6. Cladding (sheath): $T_d = T_a - \frac{r_1 q_s''}{k_s} In\left(\frac{r}{r_1}\right)$

7. Coolant: $T_h = T_b - \frac{q'''}{2hr_2} r^2$

3.5. Thermal-hydraulic parameters of MNSR Channel Assembly.

The thermal-hydraulic parameters used to simulate the mathematical model of temperature variation equations and fuel flow in the channel are given in

Table 3.1.Thermal-hydraulic parameters of the MNSR Channel Assembly[4, 13, 18]

P_c- Total Channel Power range = 0 – 30 kW.	$\acute{m}$- mass flow rate = 0.448 kg/s
$\acute{c}_p$- specific heat at constant pressure = 1.4717 kJ/kgK	T_i - inlet temperature = 24.5^0C.
T_e- exit temperature = 70.0^0C.	z- axial axis range = 0 – 0. 23 m.
H- core height = 0.23 m.	R- radius of reactor core = 0.115 m.
R'- core radius including the reflector = 0.138 m.	H'- core height including the reflector = 0.276 m.
h_c - heat transfer coefficient = 15 W/m^2K.	s- heated perimeter =0.391 m.
r_c - radius of the cladding = 0.00275 m	r_o - radius of the fuel = 0.00215 m
k_c – thermal conductivity of the cladding, W/m^0C =15.	k_f - thermal conductivity of the fuel, W/m^0C = 0.15.
k_g - conductivity of the pure gases = 5 W/mK.	P_i- surface contact pressure, N/m^2 =1.96 Psi.
-root-mean square of contact material roughness = 0.37.	$\delta_f + \delta_c$, m- temperature jump distances for gas, helium = 10x10^{-6}
δ_1, δ_2- surface roughness of the interface material, m = 0.37 each.	T_a-temperature at the inner surface of cladding= 86 ℃.
Q – power density = 30 W/cm^3	T_b-temperature at the outer surface of cladding = 30 ℃.
q – heat flux. = 1628 W/cm^2	

Other constants derived for the thermal-hydraulic parameters are:

1. $\beta = \frac{\pi H}{2H'} = 1.31$
2. h_{con} = total conductance of a closed gap : $A\frac{2k_f k_c}{k_f+k_c}\frac{P_i}{H\delta^{½}} + \frac{k_g}{C(\delta_1|+\delta_2)+\delta_f+\delta_c}$ = 466K = 193 ^oC

Substituting these constants into the equations of the temperature distributions in the axial direction, the equations t_f and t_o simplifyied to:

$$T_f = \frac{T_i+T_e}{2} + \frac{T_e-T_i}{2sin\beta}\left[sin2\beta\,\frac{z}{H} + \frac{1.4581\,P_c}{H(t_e-t_i)}cos2\beta\,\frac{z}{H}\right] \quad (3.52)$$

$$T_o = \frac{T_i + T_e}{2} + \frac{T_e - T_i}{2sin\beta}\left[sin\beta\,\frac{z}{H} + \frac{2.4720P_c}{H(t_e - t_i)}\,cos2\beta\,\frac{z}{H}\right] \quad (3.53)$$

3.6. Computer simulation of axial and radial temperature profile using LabVIEW development platform.

.

To plot the governing equations (3.6), (3.10), (3.22) and (3.38) on a single graph, each data set for the relation was bundled before finally being used in the graph. The bundle function accepted a number of inputs of varying data types which produced a single output for onward processing. For the axial temperature profile, two 1-D array data type was used as input for each of the bundle functions. The main function of the bundle was to assemble a cluster from individual elements. Figure 3.3 depicts the bundle function used for the computer simulation.

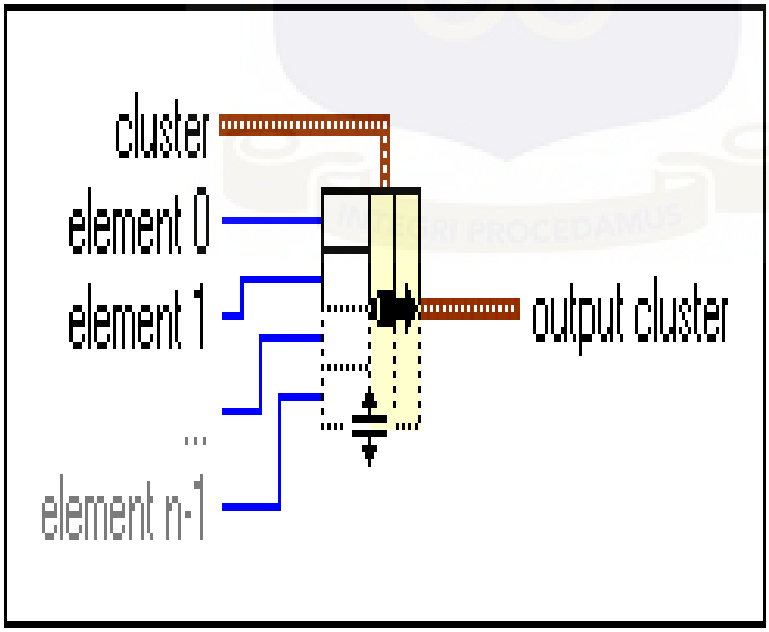

Fig 3.3 Bundle function used in LabVIEW simulation

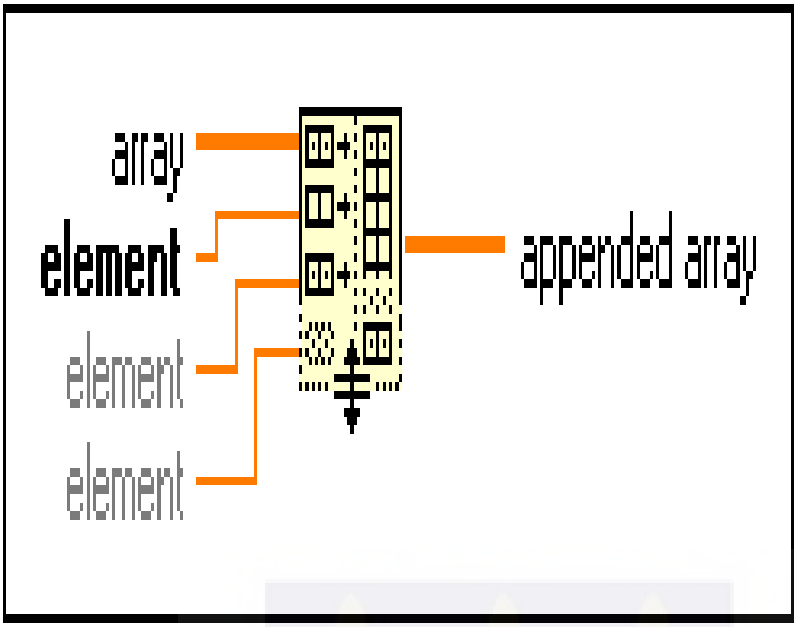

Fig 3.4 Build Array used in LabVIEW simulation

After the governing relations has been transformed using the various functions and structures the values from the bundle function for each of the governing relation were passed onto a single function known as build array function which function concatenated multiple arrays or appended elements to an n-dimensional array. The function assembled all the results of the governing relations for the axial temperature profiles for the coolant, outer surface of the cladding, fuel surface and fuel center into a single container and then passed the output for further processing to the multiple plot graphs. Figure 3.4 shows the build array function in LabVIEW.

3.6.1. Simulation of axial temperature profile

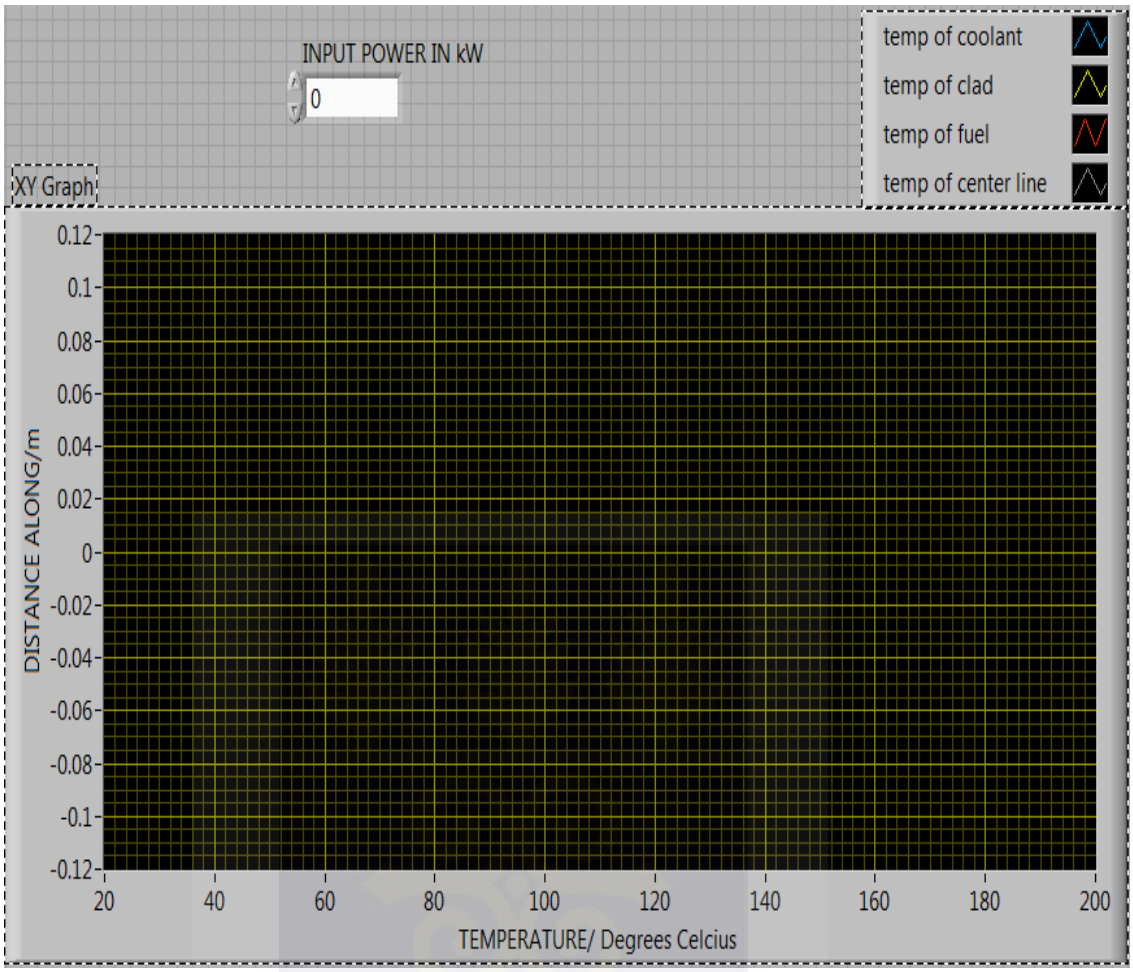

Fig 3.5 Front panel view developed in LabVIEW to display the axial temperature profiles

The front panel developed in LabVIEW to display the axial temperature profiles is shown in Figure 3.5. The temperature (in degrees celsius) was located on the abscissa of the graph and the ordinate of the graph recorded the axial length of the fuel presented in (m). The legend for the various temperature profiles was shown on the top-right corner of the graph. Finally, the numeric control button, which accepted the value of power in kilowatts was also displayed.

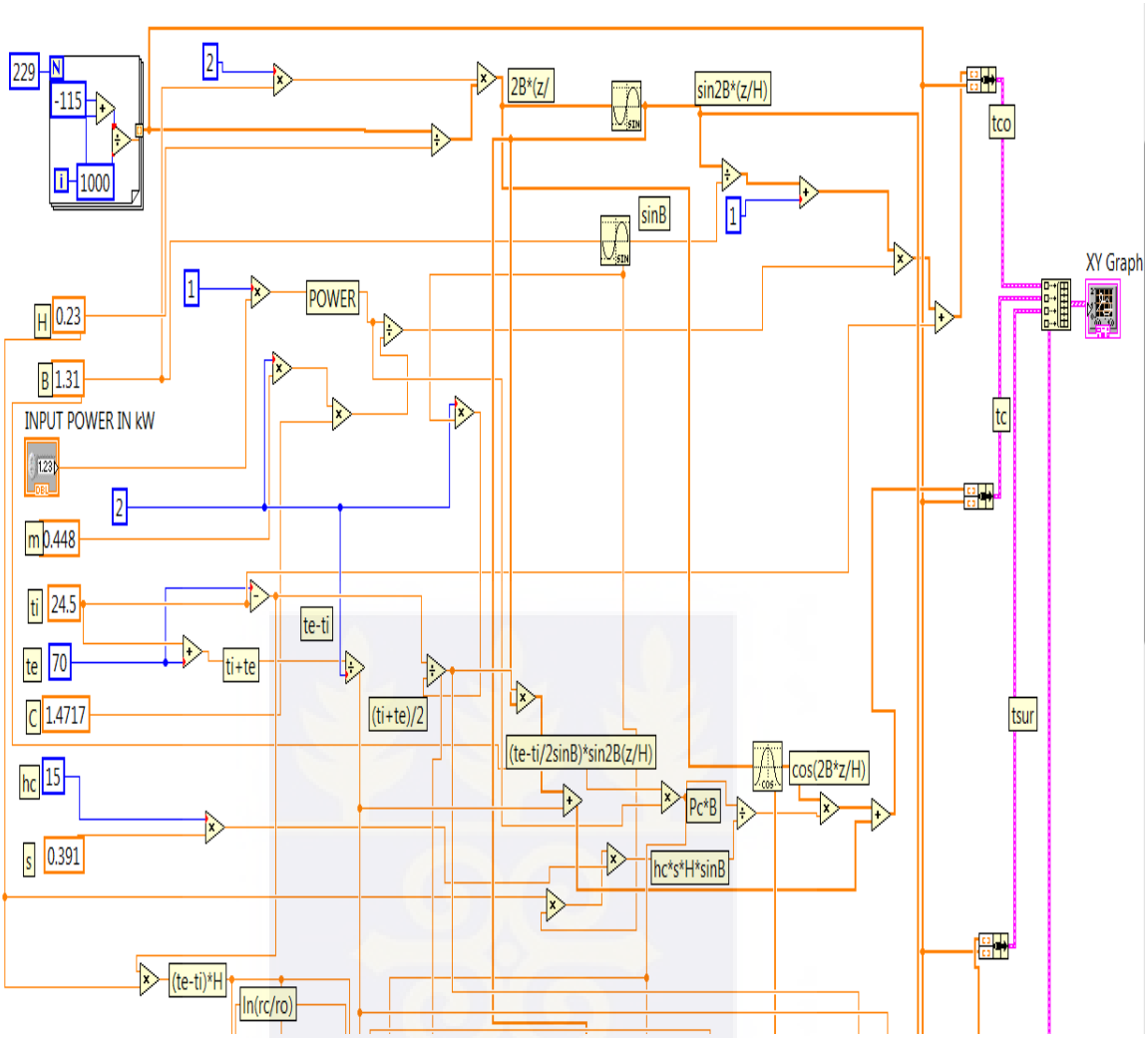

Fig 3.6 Block diagram developed in LabVIEW to display the axial temperature profiles

The block diagram for the simulation of the axial temperature profile is presented in figure 3.6. The various arithmetic functions and structures were combined so as to depict the governing relations developed for the axial temperature profile.

3.6.2. Simulation of radial temperature profile

The various arithmetic operations and structures used in axial simulator were also used in determining the radial temperature profile.

Three for loop structures were developed for the simulation and were used to generate the various intervals for the fuel meat, clad and the coolant. The governing equations were then developed using the various LabVIEW functions and structures. Figure 3.7 was the LabVIEW block diagram representation for the relations governing the radial temperature profile.

A similar approach as with that of the axial temperature profile was employed by assembling the various governing relations for the fuel meat, cladding and the coolant into three separate bundle functions and then passing them to the build array for graphical processing. The block diagram for the radial profile had temperature in degrees celsius on the ordinate of the graph and the radial distance in millimeters on the abscissa.

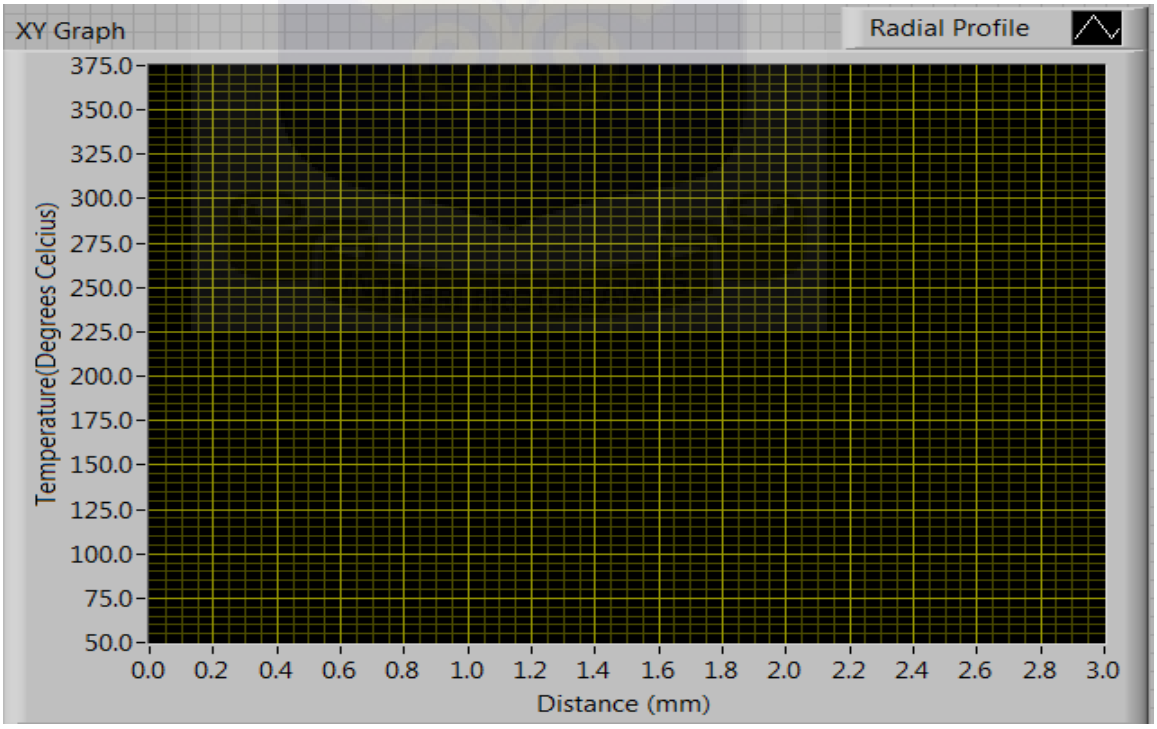

Fig 3.7 Front panel view developed in LabVIEW to display the radial temperature profiles

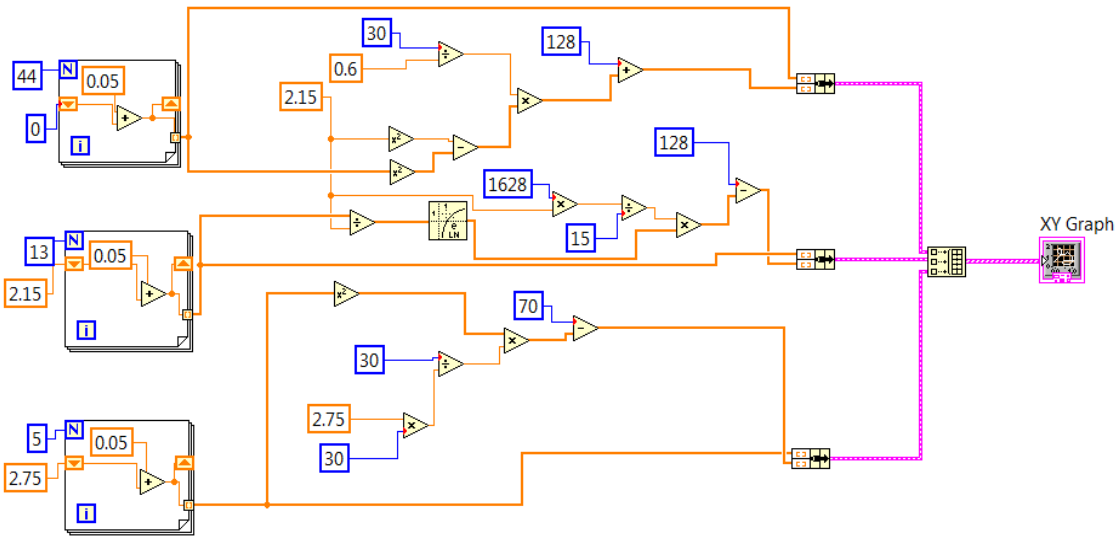

Fig 3.8 Block diagram developed in LabVIEW to display the radial temperature profiles

3.7. Validation by the MATLAB and Excel software programs

For the purpose of verifying and validating the values of temperature distribution in the components by LabVIEW both MATLAB and Excel were used.

3.7.1. MATLAB codes for axial temperature profile

Listed below are the relevant thermal-hydraulic parameters and constants used including the resulting MATLAB codes for the temperature profile in the axial direction.

```
% initialization of thermal-hydraulic parameters used in simulating in
% the axial direction.

z = [-0.115:0.005:0.115];   %   range and interval along the z-axis
T_i  =   24.5;              % inlet   temperature
T_e  = 70;                  % exit temperature
pc  = 30;                   % total channel power
cp   =1.4717;               % specific heat at constant pressure
```

```
m  =  0.448;                % mass flow rate
H   =0.23;                  % core height
Beta = 1.31;                % constant = πH/ (2H')
H = 0.276 ;                 %  height including the reflector.
hc =  15;                   % heat transfer coefficient
s = 0.391;                  % heated perimeter

%%*****************************************************************
% Computing terms in the main equation
MATLAB codes for the equations in the axial direction
VAL1 = (pc/2*m*cp) ;
VAL2 = sin (2*beta.*z/H)/sin (beta)+1;
 VAL3 = (Ti+Te)/2;
 VAL4 = (Te-Ti)/2*sin (beta);
 VAL5 = sin (2*beta.*z/H);
VAL6 =  (pc*beta*cos (2*beta.*z/H))/ (hc*s*H*sin (beta));
VAL7 = (1.4581*pc*cos (2*beta.*z/H))/ (H*(Te-Ti));
VAL8 = (2.4720*pc*cos (2*beta.*z/H))/ (H*(Te-Ti));

%-------------------------------------------------------------------
1. T = Ti+VAL1*VAL2;
2. Tc = VAL3+VAL4*VAL5+VAL6;
3. Tf = VAL3+VAL4*(VAL5+VAL7);
4. To = VAL3+VAL4*(VAL5+VAL8);
The plotting routine of the equations
1.  figure;

plot (T, z, 'm');

xlabel (' Temperature ℃.' ),  ylabel ('Axial Height');

title ('graph of axial temp. distribution in the coolant')

2. figure;

plot (Tc ,z, 'b-.');
```

xlabel (‘ Temperature ℃.’), ylabel (‘Axial Height’);

title (‘graph of temp. distribution in the outer surface of the cladding’);

3. figure;

plot (Tf ,z, 'g--');

xlabel (‘ Temperature ℃.’), ylabel (‘Axial Height’);

title (‘graph of temp. distribution in the fuel surface’);

4. figure;

plot (To ,z, 'r-*');

xlabel (‘ Temperature ℃.’), ylabel (‘Axial Height’);

title (‘graph of temp. distribution in the fuel center’);

The combined plot

figure;

plot (T, z, 'm', Tc, z,' b-.' Tf , z, 'g--', To, z,' r-*');

xlabel (‘ Temperature (Degrees Celcius)’), ylabel (‘Height of Reactor Core (m)’);

title (‘combined temp. distribution in the coolant, outer surface of the cladding, fuel surface, fuel center’);

```
%-------------------------------------------------------
%The thermal-hydraulic parameters used in simulating in
the radial direction.
%ri, rj and rk are distances from fuel element center
(m).
```

%----------

3.7.2. MATLAB codes for radial temperature profile

The relevant thermal-hydraulic parameters and constants used including the resulting MATLAB codes for the temperature profile in the radial direction were:

```
%The thermal-hydraulic parameters used in simulating in the radial direction.
%ri, rj and rk are distances from fuel element centre (mm).

ri = [0.0:0.05:2.15];      % range and interval for the fuel meat of radius 2.15 mm;
rj = [2.15:0.05:2.75];     % range and interval from the inner to outer surfaces of
cladding;
rk = [2.75:0.05:2.9];      % width of the coolant channel;
 h = 15;                   % heat transfer coefficient;
rf = 2.15;                 % radius of the fuel;
rc = 2.75;                 % width of the cladding;
 kf = 0.15;                % conductivity of the fuel;
 kc = 15;                  % conductivity of the cladding;
q   = 1628;                % heat flux;
Q = 30;                    % power density;
Ta = 86;                   % temperature at inner surface of cladding;
Tb = 30;                   % temperature at the outer surface of cladding;
```

% codes for the equations in the radial direction.

MATLAB codes for the equations in the radial direction.

1. Tf = Ta+(Q/(4*kf))*(rf.^2-ri.^2);

2. Td = Ta-((rf*q)* reallog (rj/rf)/kc);

3. Th = Tb-(Q*rk.^2)/(2*h* rc);

The plotting routine of the equations.

```
1. figure;

plot(ri,Tf,'r');

xlabel('Radial distance (mm)',ylabel('Temperature ℃');
```

title ('graph of radial temp. distribution in the fuel');

```
2. figure;

plot(rj,Tc,'g--');

xlabel('Radial distance (mm)',ylabel('Temperature ℃');
```

title ('graph of radial temp. distribution in the sheath(cladding)');

```
3. figure;

plot(rk,Th,'b-');

xlabel('Radial distance (mm)',ylabel('Temperature ℃');
```

title ('graph of radial temp. distribution in the coolant');

The combined plot

```
figure;

plot(ri,Tf,'r', rj,Td,'g--', rk,Th,'b-');

xlabel('Radial Distance (mm)',ylabel('Temperature
(Degrees
```

Celcius)');

title (' Combined radial temp. distribution demarcating clearly each region ');

legend ('Fuel Rod',' Cladding', 'Coolant')

3.7.3 Excel spreadsheet for axial temperature profile

(1) In cells A1, B1, C1, D1 , E1 , F1, G1, H1 and I1 were entered Te, pc, beta, m, cp, H, te, hc and s respectively.

(2) In cells A2, B2, C2, D2, E2, F2, G2, H2, I2 and J2 the following values were entered respectively:

24.5, 30, 1.31, 0.448, 1.4717, 0.23, 70, 15, 0.391 and 0.005 for the step size

(3) Name cells A5, B5, C5, D5 and E5 as z, T, T_c, T_f *and* T_o respectively.

(4) Entered in cell A6 the value -0.115 and Enter pressed. Place the cell highlight in cell A6 and highlight the block of cells A6 to A52 by holding down the mouse button

and wiping the highlight down to cell A52. Click the Edit command on the Command bar and point at Fill from the drop-down menu. Select Series from the next drop-down menu and accept the default Step value of 0.005 by clicking OK in the series window. This yielded -0.115, -0.11, -0.105, -0.1, -0.095, …, 0.115.

(5) In the cell B6 was entered the formula

= $A$2+($B$2/(2*$D$2*$E$2))*((SIN(2* $C$2*A6/$F$2)/SIN($C$2)+1))

(6) The cell highlight was placed in cell B6. The Edit command was clicked and Copy was selected from the drop-down menu. The contents of cell B6 were copied to the clipboard. Now the cell highlight was placed in cell B7 and the block cells from B7 to B52 were highlighted. The Edit command was clicked again but now Paste was selected from the drop- down menu.

The result was 24.8825, 25.3376, 25.8637, 26.4592, 27.1221,…, 70.0013.

(7) Similarly, in the cells C6, D6 and E6 the under-listed formulas for T_c, T_f and T_o were entered respectively and the processes in (7) were repeated.

3.7.4. Excel code for the axial temperature distribution

T =$A$2+($B$2/(2*$D$2*$E$2))*((SIN(2* $C$2*A6/$F$2)/SIN($C$2)+1));

T_c=(($A$2+$G$2)/2)+(G2$A$2)*(SIN(2*$C$2*A6/$F$2))/(2*SIN($C$2))+($B$2*$C$2*COS(2*$C$2*A6/$F$2))/($H$2*$I$2*$F$2*SIN($C$2));

T_f = (($A$2+$G$2)/2)+

((G2$A$2)/(2*SIN($C$2)))*(SIN(2*$C$2*A6/$F$2)+((1.4581*$B$2*COS(2*$C$2*A6/$F$2)))/($F$2*($G$2-$A$2)));

T_o =(($A$2+$G$2)/2)+((G2$A$2)/(2*SIN($C$2)))*(SIN(2*$C$2*A6/$F$2)+((2.472*$B$2*COS(2*$C$2*A6/$F$2)))/($F$2*($G$2-$A$2)));

3.7.5. Excel spreadsheet for radial temperature profile

(1) In cells A1, B1, C1, D1 ,E1 and F1 were entered ri, rj, rk, Tf, Td and Th respectively.

(2) In cells M2, M3, M4, M5, M6, M7, M8, M9 and M10 were named h, rf, rc, kc, kf, q, Q, Ta and Th respectively.

(3) Cells N2 to N10 contained the corresponding values of the hydraulic parameters in (3) above: 15, 2.15, 2.75, 15, 0.15, 1628, 30, 86, and 3.0

(4) In cells A1, B1 and C1 were entered ri, rj and rk. highlight the block of cells A2 to A45 by holding down the mouse button and wiping the highlight down to cell A45. Click the Edit command on the Command bar and point at Fill from the drop-down menu. Select Series from the next drop-down menu and accept the default Step value of 0.05 by clicking OK in the series window. This yielded 0.00, 0.05, 0.10, 0.15, 0.20 ,…, 2.15.

(5) Same process was carried out in columns B and C starting with the initial values of 2.15 and 2.75 in cells B2 and C2 respectively.

(6) In the cell A45 was entered the formula T_f:

=$N$9+ ($N$8/(4*$N$6))*(($N$3^2) - (A45^2))

(7) The cell highlight was placed in cell A45. The Edit command was clicked and Copy was selected from the drop-down menu. The contents of cell A45 were copied to the clipboard. Now the cell highlight was placed in cell A44 and the block cells from A44 to A2 were highlighted. The Edit command was clicked again but now Paste was selected from the drop- down menu.

The result was 317.125, 317.000, 316.625, 316.000, 315.125, …, 86.000.

(8) Similarly, in the cells B2 and C2 were entered the under-listed formulas for T_d and T_h respectively and the processes in (7) were repeated.

3.7.6. Excel code for the radial temperature distribution

T_f= $N$9+ ($N$8 / (4*$N$6))*(($N$3^2) - (A2^2));

T_c= ($N$9) - ((($N$3*$N$7) / $N$5)*L N (B2 / $N$3));

T_h= ($N$10) - (($N$8 / (2*$N$2*$N$4))*(C2^2));

Excel has been used to calculate and analyze the temperature values at discrete points in each of the components of the reactor core. Tables 4.2 and 4.7

This was done to ascertain the phenomenon and structural behavior of the reactor core under normal operation using different procedures. In table 4.2 the location of maximum temperatures in the four components in the axial direction were marked with asterisk. This is displayed in table 4.3

CHAPTER FOUR

RESULTS AND DISCUSSIONS

4.1. LabVIEW Simulation of the Mathematical models of temperature distribution in the coolant, outer surface of cladding, fuel surface and fuel center.

Shown in figures 4.1 and 4.3 are the plots of the equations in the axial and radial directions using LabVIEW for the given sets of initial conditions. The combined plots of temperature profile in the rector components in the axial direction using LabVIEW and MATLAB were very identical. The LabVIEW and MATLAB plots of temperature profile in the components in the radial direction were also similar. Compare figures 4.1 with 4.8 for axial plots and 4.3 with 4.12 for the radial plots.

LabVIEW Simulation (Axial direction) FRONT PANEL

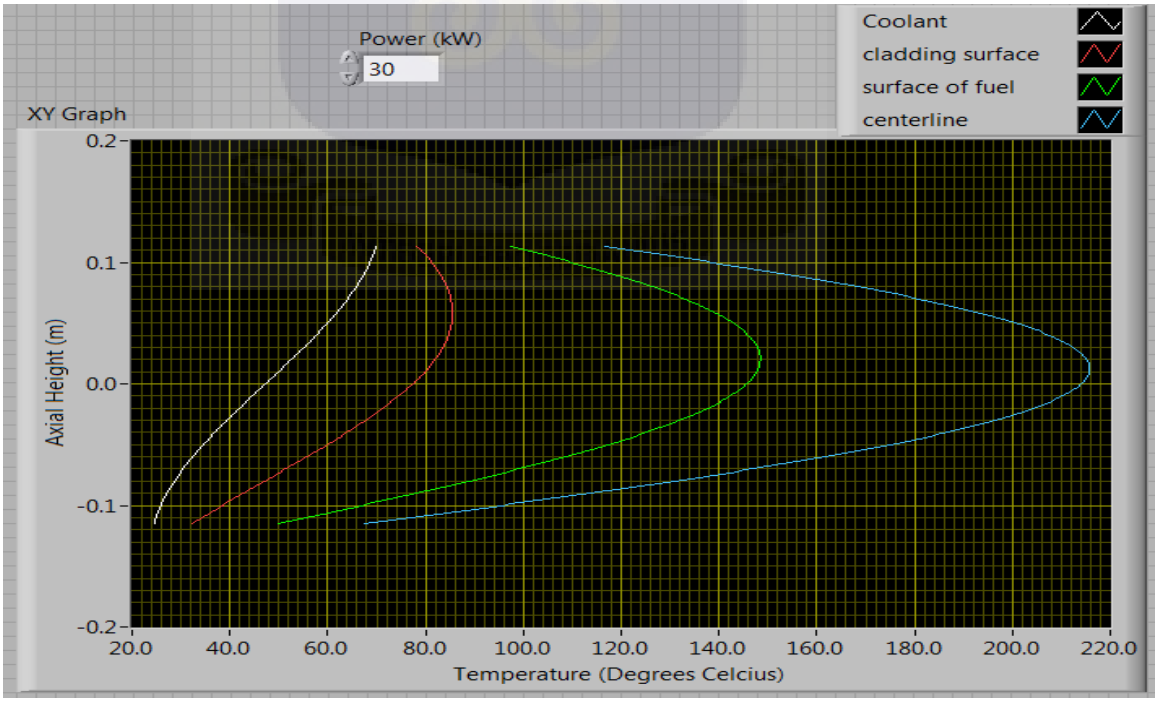

Fig.4.1. Plot of temperature in degrees celsius against axial height in m. with P_C = 30 kW

Figure 4.2 are the graphs that were the visual simulation of the temperature profile in the four components in the axial direction with varying values of P_C (i) 5 kW, (ii) 10 kW, (iii) 15 kW and (iv) 25 kW

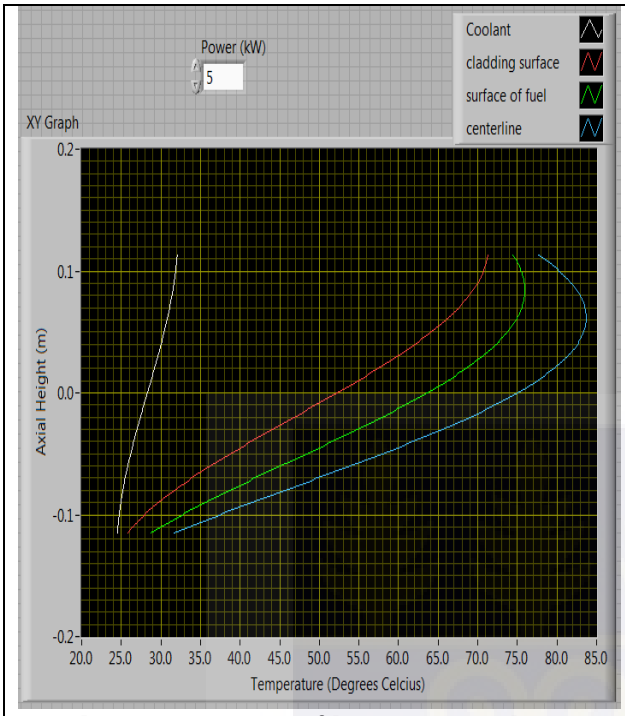

Axial Temperature Profile at Power=5kW

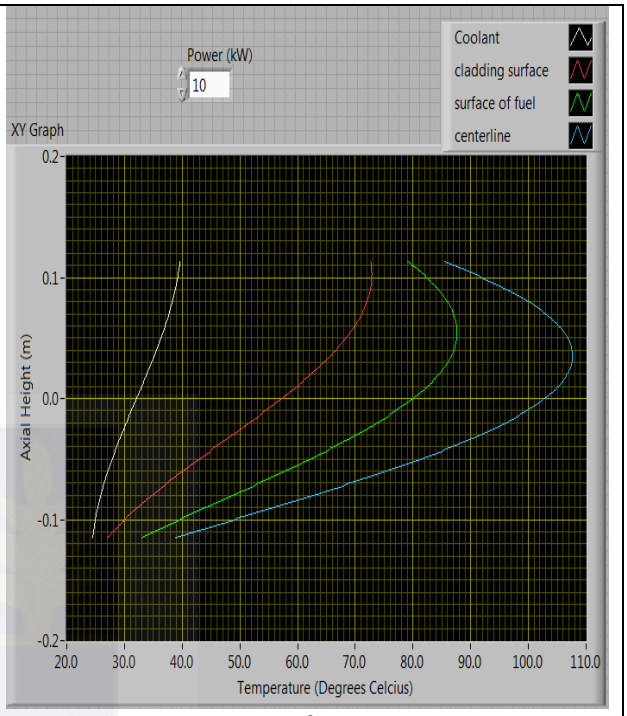

Axial Temperature Profile at Power=10kW

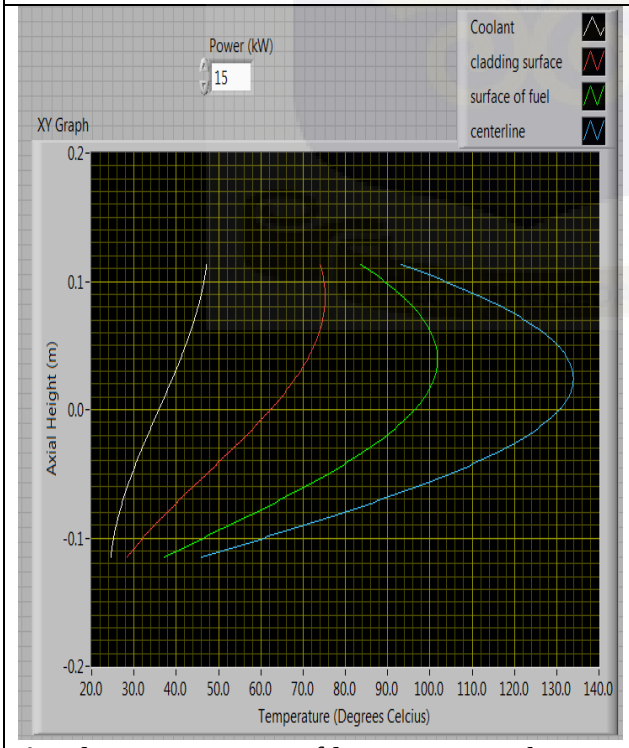

Axial Temperature Profile at Power=15kW

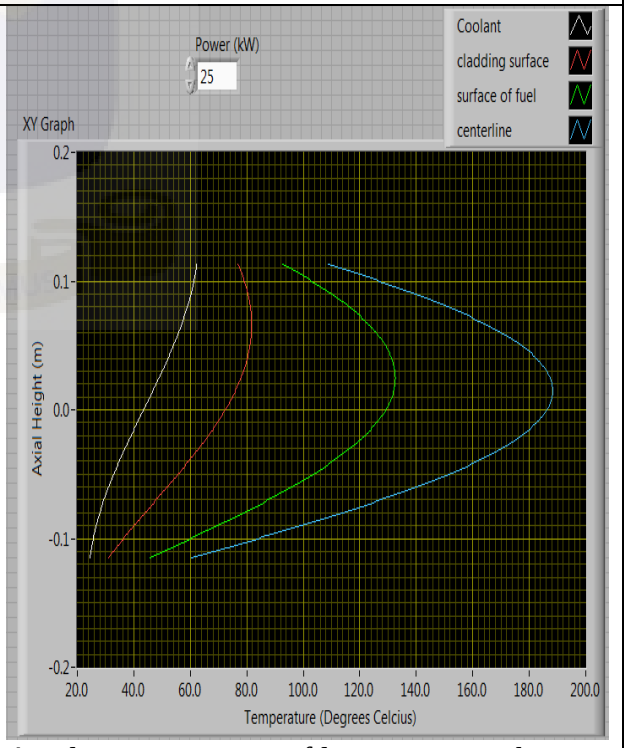

Axial Temperature Profile at Power=25kW

Fig 4.2 Plot of temperature profile in the reactor components for values of (i) 5 kW (ii) 10 kW (iii) 15 kW and (iv) 25 kW

LabVIEW simulation (radial direction) FRONT PANEL

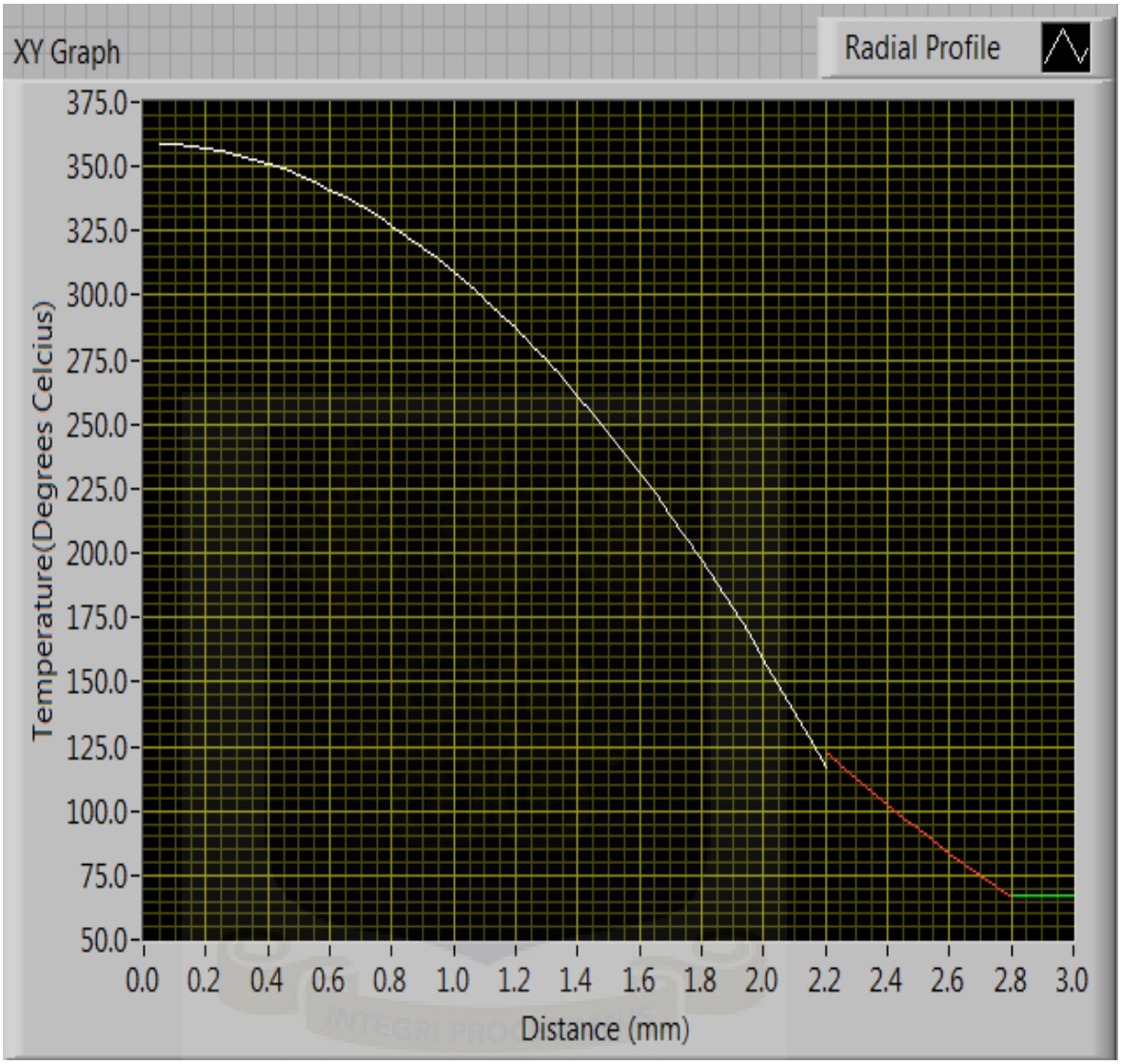

Fig.4.3 Plots of temperature in degrees celcius against radial distance in mm

4.2. Temperature profile of the coolant, cladding and fuel element.

The axial temperature distribution of the coolant, outer surface of the cladding, surface of the fuel and fuel center were obtained using eqns. (3.6), (3.10), (3.22) and (3.38) respectively and the corresponding results presented in Table 4.1

The radial temperature distribution in the fuel, cladding and the coolant were also constructed using eqns. (3.46), (3.49) and (3.51) and the data are shown in Tables 4.4, 4.5 and 4.6 respectively.

Table 4.1 Axial temperature distribution in the coolant (T), outer surface of the cladding (T_c), fuel surface (T_f) and fuel center (T_0) using MATLAB for:

T = $\frac{T_i - T_e}{2} + \frac{T_e - T_i}{2sin\beta} sin2\beta \frac{z}{H}$, and z = 0.0 to 0.115 m

$T_c = \frac{T_i + T_e}{2} + \frac{T_e - T_i}{2sin\beta} sin2\beta \frac{z}{H} + \frac{1}{h_c s} \frac{P_c}{H} \frac{\beta}{sin\beta} cos2\beta \frac{z}{H}$, and z = 0.0 to 0.115m

$T_f = \frac{T_i + T_e}{2} + \frac{T_e - T_i}{2sin\beta}$ [sinβ$\frac{z}{H}$ + ($\frac{1}{\gamma} + \frac{\beta}{2\pi k_c} \frac{P_C}{(T_e - T_i)H}$ In $\frac{r_c}{r_o} + \frac{\beta}{\pi r_o h_{con}} \frac{P_C}{(T_e - T_i)H}$) cos2β$\frac{z}{H}$, and z = 0.0 to 0.115 m

$T_o = \frac{T_i + T_e}{2} + \frac{T_e - T_i}{2sin\beta}$ [sinβ$\frac{z}{H}$ + ($\frac{1}{\gamma} + \frac{\beta}{2\pi k_c} \frac{P_C}{(T_e - T_i)H}$ In $\frac{r_c}{r_o} + \frac{\beta}{\pi r_o h_{con}} \frac{P_C}{(T_e - T_i)H} + \frac{\beta}{2\pi k_f} \frac{P_C}{(T_e - T_i)H}$) cos2β$\frac{z}{H}$], and z = 0.0 to 0.115 m

Table 4.1 The axial temperature distribution in the coolant, outer surface of cladding, fuel surface and fuel centerline using MATLAB

Height of reactor core(m)	Temperature ℃			
Z	**T**	T_c	T_f	T_o
-0.115	24.500	33.788	49.703	66.177
-0.110	24.883	35.791	55.075	75.036
-0.105	25.338	37.830	60.422	83.805
-0.100	25.864	39.901	65.726	92.456
-0.095	26.459	41.996	70.970	100.960
-0.090	27.122	44.107	76.137	109.289
-0.085	27.850	46.229	81.210	117.418
-0.080	28.642	48.354	86.174	125.319
-0.075	29.493	50.476	91.011	132.967
-0.070	30.402	52.586	95.706	140.336
-0.065	31.366	54.68	100.244	147.404
-0.060	32.381	56.750	104.610	154.147
-0.055	33.444	58.789	108.790	160.544
-0.050	34.553	60.790	112.770	166.573
-0.045	35.702	62.747	116.538	172.214
-0.040	36.889	64.654	120.081	177.451
-0.035	38.109	66.505	123.389	182.266
-0.030	39.360	68.293	126.449	186.642
-0.025	40.635	70.013	129.252	190.567
-0.020	41.932	71.660	131.790	194.026
0.015	43.247	73.227	134.052	197.010
--0.010	44.574	74.710	136.034	199.508
-0.005	45.910	76.103	137.728	201.512
0.000	47.251	77.403	139.128	203.016

0.005	48.591	78.606	140.230	204.015
0.010	49.927	79.83	141.031	204.505
0.015	51.255	81.589	141.528	204.485
0.020	52.569	82.364	141.718	203.955
0.025	53.866	83.026	141.603	202.918
0.030	55.142	83.572	141.181	201.375
0.035	56.392	84.000	140.455	199.332
0.040	57.612	84.308	139.427	196.796
0.045	58.799	84.497	138.099	193.775
0.050	59.949	84.564	136.477	190.279
0.055	61.057	84.511	134.566	186.320
0.060	62.120	84.337	132.371	181.909
0.065	63.136	84.042	129.900	177.061
0.070	64.099	83.629	127.162	171.792
0.075	65.008	83.097	124.164	166.120
0.080	65.860	82.449	120.916	160.062
0.085	66.651	81.687	117.430	153.638
0.090	67.379	80.813	113.716	146.869
0.095	68.042	79.830	109.787	139.777
0.100	68.638	78.742	105.655	132.384
0.105	69.164	77.551	101.333	124.716
0.110	69.619	76.263	96.836	116.797
0.115	70.001	75.025	92.178	108.652

Table 4.2. Excel calculation of axial temperature distribution in the fuel channel using spreadsheet.

T_i	pc	Beta	m	cp	H	T_e	hc	s
24.5	30	1.31	0.448	1.4717	0.23	70	15	0.391

z	T	T_c	T_f	T_o
-0.115	24.5	32.27506	49.87802	67.5248
-0.11	24.88252	34.30342	55.63264	77.01495
-0.105	25.33758	36.37377	61.36007	86.40858
-0.1	25.86372	38.4794	67.04175	95.67521
-0.095	26.45921	40.61346	72.65924	104.7848
-0.09	27.12213	42.76906	78.19432	113.7078
-0.085	27.85034	44.93918	83.62904	122.4152
-0.08	28.64146	47.1168	88.94578	130.8789
-0.075	29.49294	49.29485	94.12729	139.0713
-0.07	30.402	51.46627	99.15678	146.966
-0.065	31.36571	53.62402	104.0179	154.5373
-0.06	32.38094	55.76109	108.6949	161.7606
-0.055	33.44439	57.87056	113.1727	168.6125
-0.05	34.55262	59.94558	117.4367	175.0709
-0.045	35.70203	61.97944	121.473	181.1147
-0.04	36.88889	63.96552	125.2686	186.7243
-0.035	38.10936	65.89739	128.8112	191.8816
-0.03	39.35948	67.76878	132.0893	196.5699
-0.025	40.63518	69.57363	135.0922	200.7738
-0.02	41.93235	71.30608	137.8102	204.4799
-0.015	43.24676	72.96051	140.2345	207.676
-0.01	44.57416	74.53156	142.3573	210.3519
-0.005	45.91023	76.01413	144.1716	212.4988
0	47.25066	77.40341	145.6716	214.1098
0.005	48.59108	78.6949	146.8524	215.1796
0.01	49.92716	79.88441	147.7102	215.7048
0.015	51.25456	80.96808	148.2421	215.6836

0.02	52.56897	81.94239	148.4465	215.1162
0.025	53.86613	82.8042	148.3227	214.0044
0.03	55.14184	83.55069	147.8712	212.3518
0.035	56.39195	84.17945	147.0933	210.1637
0.04	57.61242	84.68845	145.9915	207.4472
0.045	58.79929	85.07603	144.5696	204.2112
0.05	59.9487	85.34093	142.832	200.4662
0.055	61.05693	85.4823	140.7844	196.2243
0.06	62.12038	85.49967*	138.4335	191.4992
0.065	63.1356	85.39299	135.7869	186.3062
0.07	64.09931	85.16261	132.8531	180.6623
0.075	65.00838	84.80927	129.6417	174.5858
0.08	65.85986	84.33412	126.1631	168.0962
0.085	66.65098	83.7387	122.4286	161.2147
0.09	67.37918	83.02494	118.4502	153.9637
0.095	68.04211	82.19516	114.2409	146.3665
0.1	68.6376	81.25204	109.8144	138.4479
0.105	69.16373	80.19865	105.185	130.2335
0.11	69.61879	79.0384	100.3676	121.7499
0.115	70.00132*	77.77506	95.37802	113.0248

Table 4.3. Locations of maximum temperatures in the components of the fuel rod

COMPONENT	AXIAL HEIGHT(Z)	TEMPERATURE (^{o}C)
Coolant	0.115m	70.00
Surface of clad.	0.06m	85.50
Fuel surface	0.02m	148.45
Fuel center	0.01m	215.70

Table 4.4 Radial temperature distribution in the fuel using MATLAB

$T_f = T_a + \frac{q'''}{4k_f}(r_1{}^2 - r^2)$, (for r = 0.00 to 2.15 mm).

r	0.00	0.05	0.10	0.15	0.20	0.25	0.30	0.35
T	317.13	371.00	316.63	316.00	315.13	314.00	312.63	311.00
r	0.40	0.45	0.50	0.55	0.60	0.65	0.70	0.75
T	309.13	307.00	304.63	302.00	299.13	296.00	292.63	289.00
r	0.80	0.85	0.90	0.95	1.00	1.05	1.10	1.15
T	2.85.13	281.00	276.63	272.00	267.13	262.00	256.63	251.00
r	1.20	1.25	1.30	1.35	1.40	1.45	1.50	1.55
T	245.13	239.00	232.63	226.00	219.13	212.00	204.63	197.00
r	1.60	1.65	1.70	1.75	1.80	1.85	1.90	1.95
T	189.13	181.00	172.63	164.00	155.13	146.00	136.63	127.00
r	2.00	2.05	2.10	2.15				
T	117.13	107.00	96.63	86.00				

Table 4.5 The radial temperature distribution in the sheath (cladding) using MATLAB

$T_d = T_a - \frac{r_1 q_s''}{k_s} \ln(\frac{r}{r_1})$, (for r = 2.15 to 2.75 mm)

r	2.15	2.20	2.25	2.30	2.35	2.40	2.45
T	86.00	80.64	75.39	70.26	65.24	60.33	55.52
r	2.50	2.55	2.60	2.65	2.70	2.75	
T	50.81	46.19	41.65	37.21	32.85	28.57	

Table 4.6 The radial temperature distribution in the coolant using MATLAB

Coolant: $T_h = T_b - \frac{q'''}{2hr_2}$, (for r = 2.75 to 2.90 mm)

r	2.75	2.80	2.85	2.90
T	27.2500	27.1491	27.0464	26.9418

Table 4.3 was teased out from the structured excel Table 4.2 to highlight on the positions of maximum temperatures in each component in the axial direction and it showed the order in which the maximum temperatures were attained in the four components.

Temperature distribution in the radial direction of the fuel, clad and coolant by the excel program is shown in Table 4.7

Table 4.7. Radial temperature distribution in the fuel, clad and coolant using the spreadsheet

rf	rd	rh	T_f	T_d	T_h
0.00	2.15	2.75	**317.1250**	**86.0000**	**27.2500**
0.05	2.20	2.80	**317.0000**	**80.6355**	**27.1491**
0.10	2.25	2.85	**316.6250**	**75.3915**	**27.0464**
0.15	2.30	2.90	**316.0000**	**70.2628**	**26.9418**
0.20	2.35	2.95	**315.1250**	**65.2444**	**26.8355**
0.25	2.40	3.00	**314.0000**	**60.3317**	**26.7273**
0.30	2.45		**312.6250**	**55.5202**	
0.35	2.50		**311.0000**	**50.8060**	
0.40	2.55		**309.1250**	**46.1851**	
0.45	2.60		**307.0000**	**41.6540**	
0.50	2.65		**304.6250**	**37.2091**	
0.55	2.70		**302.0000**	**32.8474**	
0.60	2.75		**299.1250**	**28.5657**	
0.65			**296.0000**		
0.70			**292.6250**		
0.75			**289.0000**		
0.80			**285.1250**		
0.85			**281.0000**		
0.90			**276.6250**		
0.95			**272.0000**		
1.00			**267.1250**		
1.05			**262.0000**		
1.10			**256.6250**		
1.15			**251.0000**		
1.20			**245.1250**		
1.25			**239.0000**		
1.30			**232.6250**		
1.35			**226.0000**		
1.40			**219.1250**		

1.45	**212.0000**
1.50	**204.6250**
1.55	**197.0000**
1.60	**189.1250**
1.65	**181.0000**
1.70	**172.6250**
1.75	**164.0000**
1.80	**155.1250**
1.85	**146.0000**
1.90	**136.6250**
1.95	**127.0000**
2.00	**117.1250**
2.05	**107.0000**
2.10	**96.6250**
2.15	**86.0000**

4.3. The plots of temperature profile of the fuel-channel elements in the axial direction.

A plot by MATLAB of the axial temperature distribution in the coolant, cladding, fuel surface and fuel center using Table 4.1 is illustrated by Figures 4.4, 4.5, 4.6, 4.7 and 4.8.

Figure 4.4 is a plot of temperature profile of the coolant in the axial direction. The trend approximated to a straight line graph of positive gradient. The only variations were identified at the inlet region were the rise in temperature was more rapid and towards the exit where a more rapid reduction in temperature was experienced. The increase in temperature was steady between these two regions.

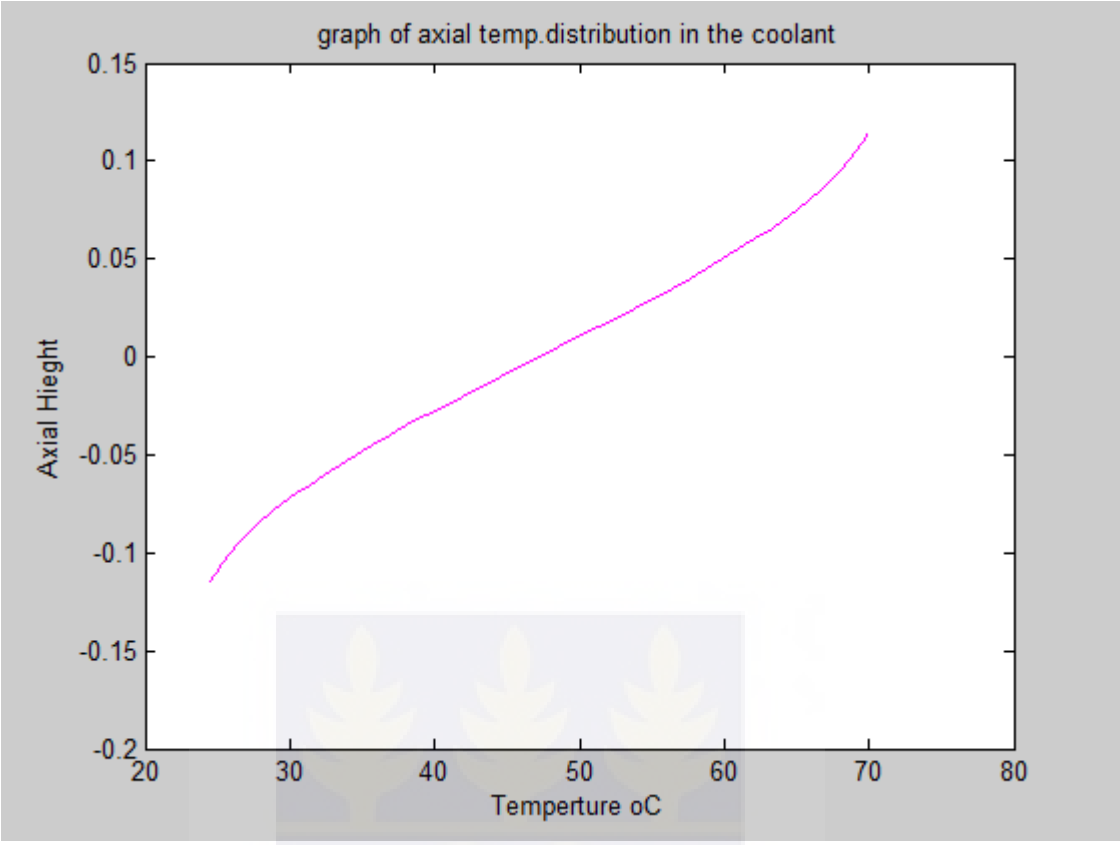

Fig.4.4. Axial temperature distribution in the coolant

Figure 4.5 shows the trend of temperature profile in the outer surface of the cladding. The graph depicted a steady rise in temperature until the maximum point was reached. Thereafter there was a rapid decrease in temperature to the reactor exit. The shape of the graph is hyperbolic.

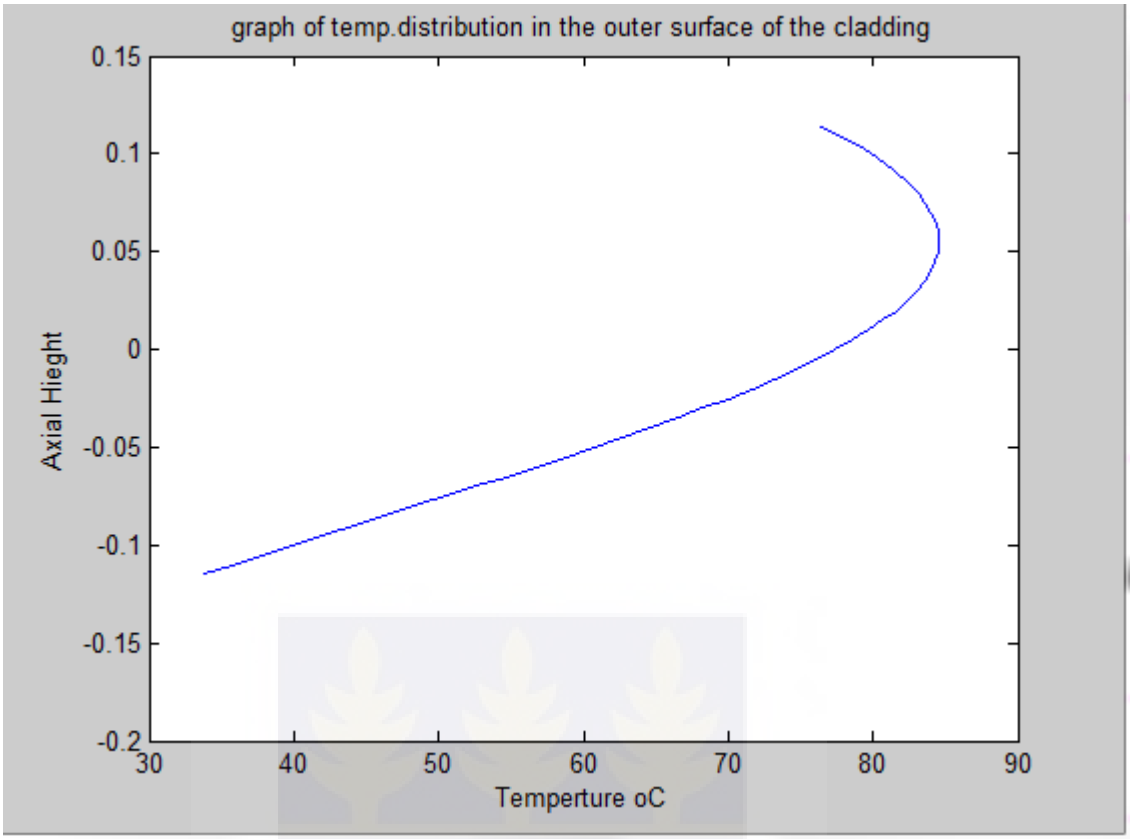

Fig.4.5 Axial temperature distribution in the outer surface of the cladding

Figure 4.6 is the plot of temperature profile in the surface of the fuel. The shape was hyperbolic and the trend was also similar to that of the temperature profile in the outer surface of the cladding.

The temperature profile at the fuel center is shown in figure 4.7. Although the shape and the trend were similar to the temperature profiles in the outer surface of the cladding and surface of the fuel, its hyperbolic shape was much more symmetrical.

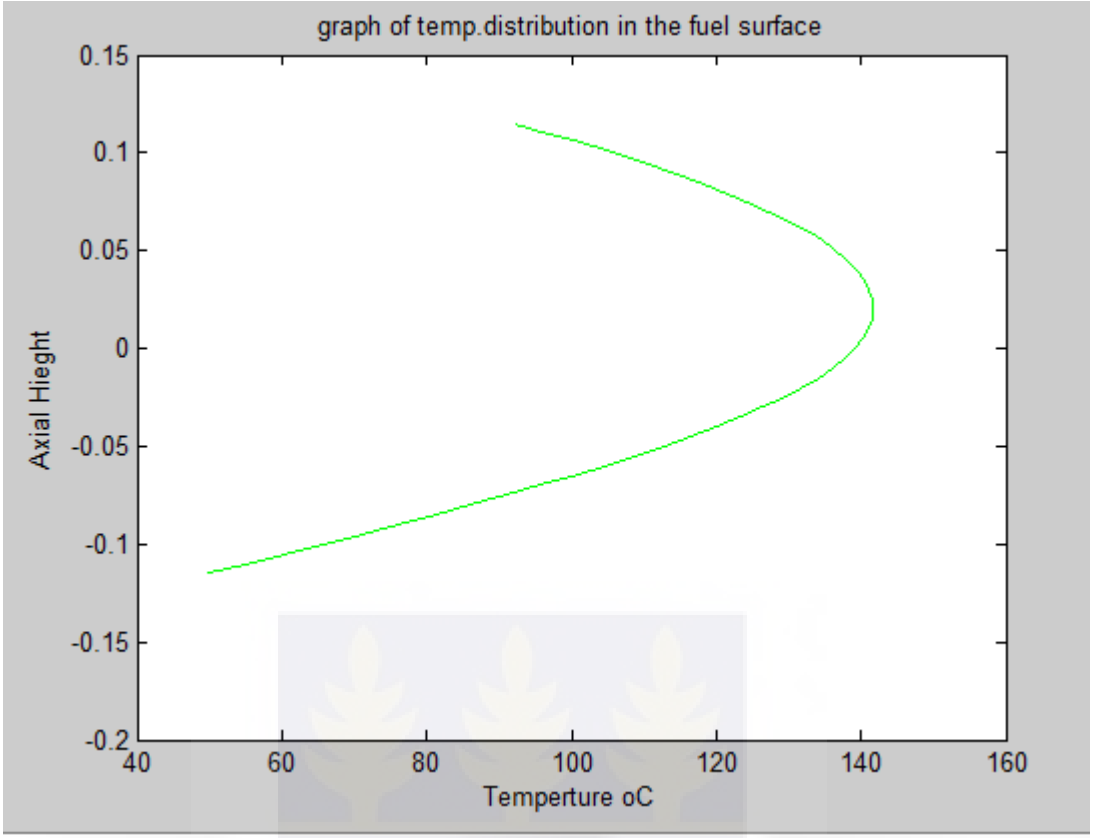

Fig 4.6 The axial temperature distribution in the fuel surface

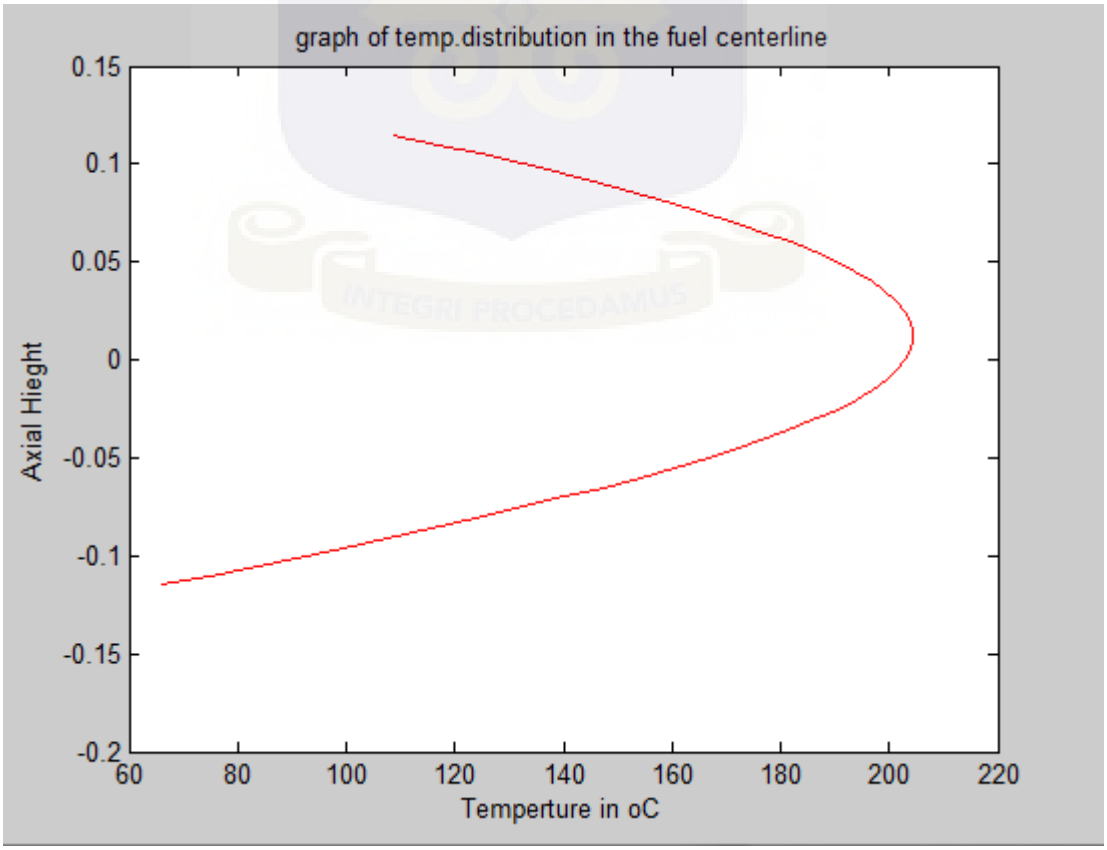

Fig.4.7. The axial temperature distribution along the fuel center

Figure 4.8 is the combined plots of the temperature profile in all the four components in the axial direction for comparison and analysis.

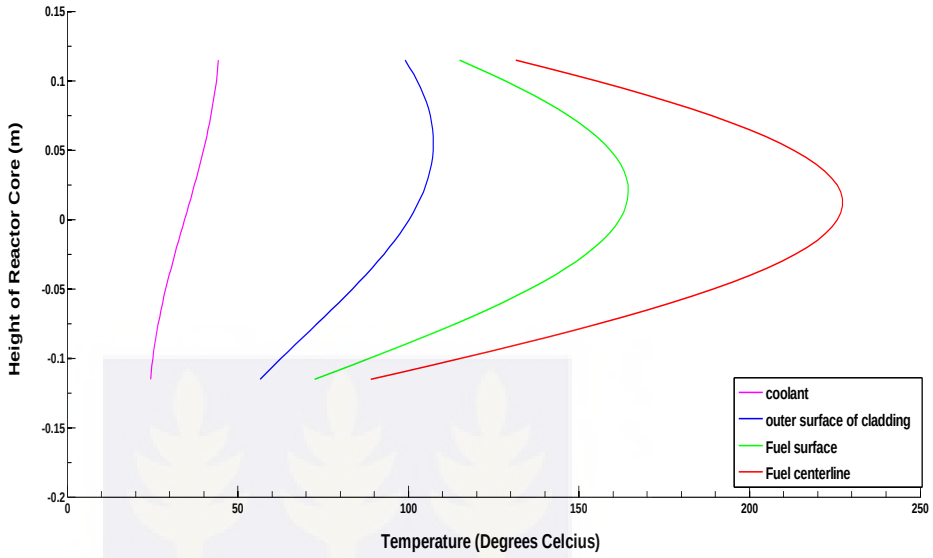

Fig.4.8.Combined temperature distribution in the axial direction in a fuel channel (coolant, outer surface of the cladding, fuel surface and fuel center).

4.4. The plots of temperature profile of the fuel-channel elements in the radial direction

A plot by MATLAB of radial temperature distribution in the fuel, cladding and coolant using tables 4.4, 4.5 and 4.6.

Figure 4.9 is the plot of temperature profile in the fuel at the radial direction. The trend was parabolic while the temperature axis acted as the line of symmetry.

Figure 4.10 shows the temperature profile in the clad. The profile followed a straight line graph of negative gradient descent.

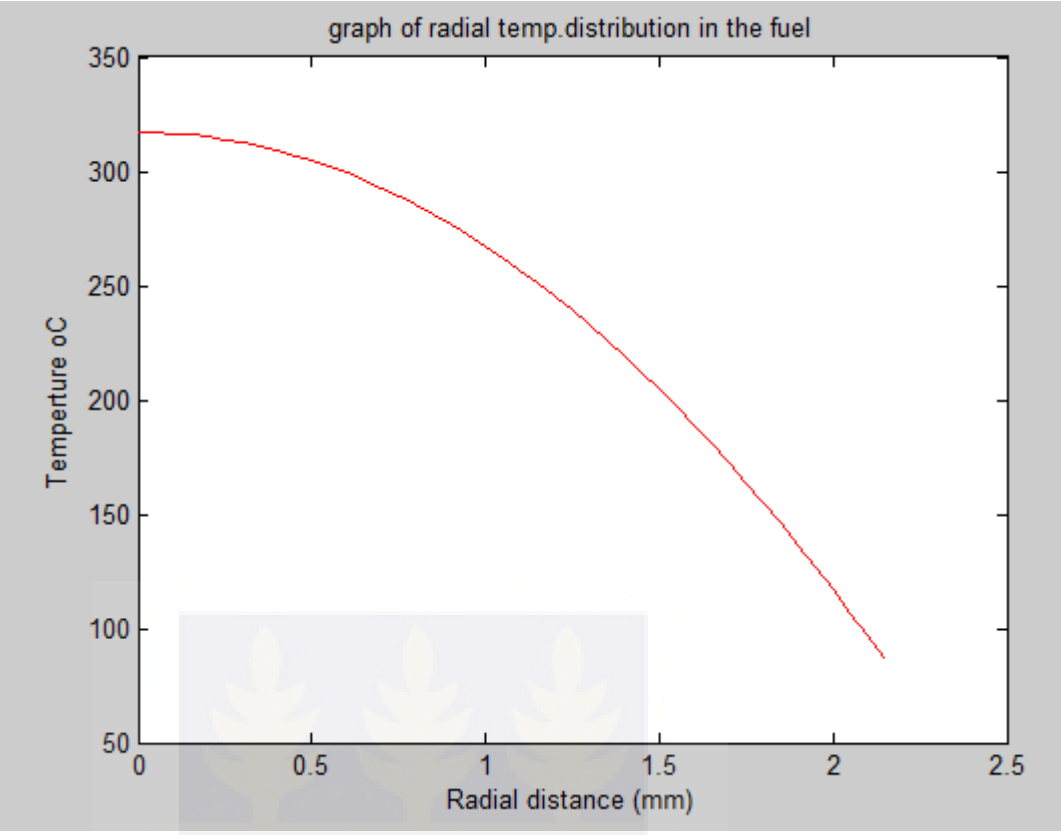

Fig. 4.9 Radial temperature distribution in the fuel

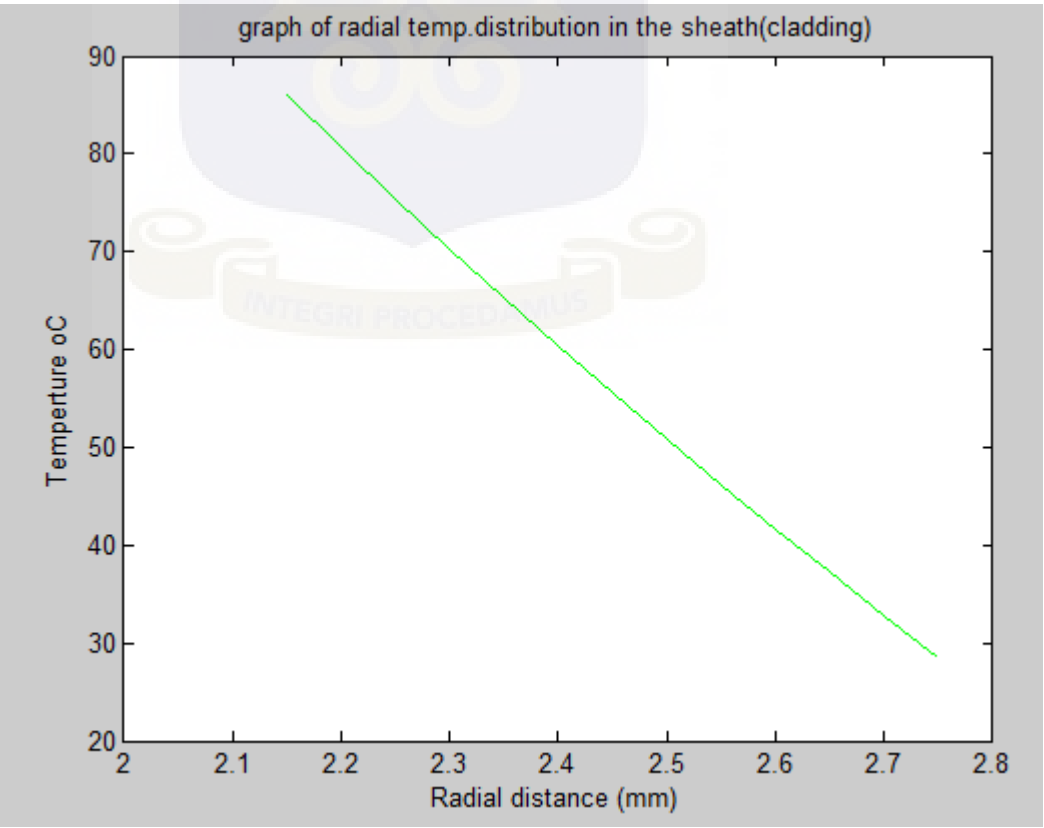

Fig 4.10 .Radial temperature distribution in the sheath (cladding)

The plot of temperature profile in the coolant in the radial direction is shown in figure 4.11. The trend was approximately a horizontal straight line. This trend described very small changes in temperature.

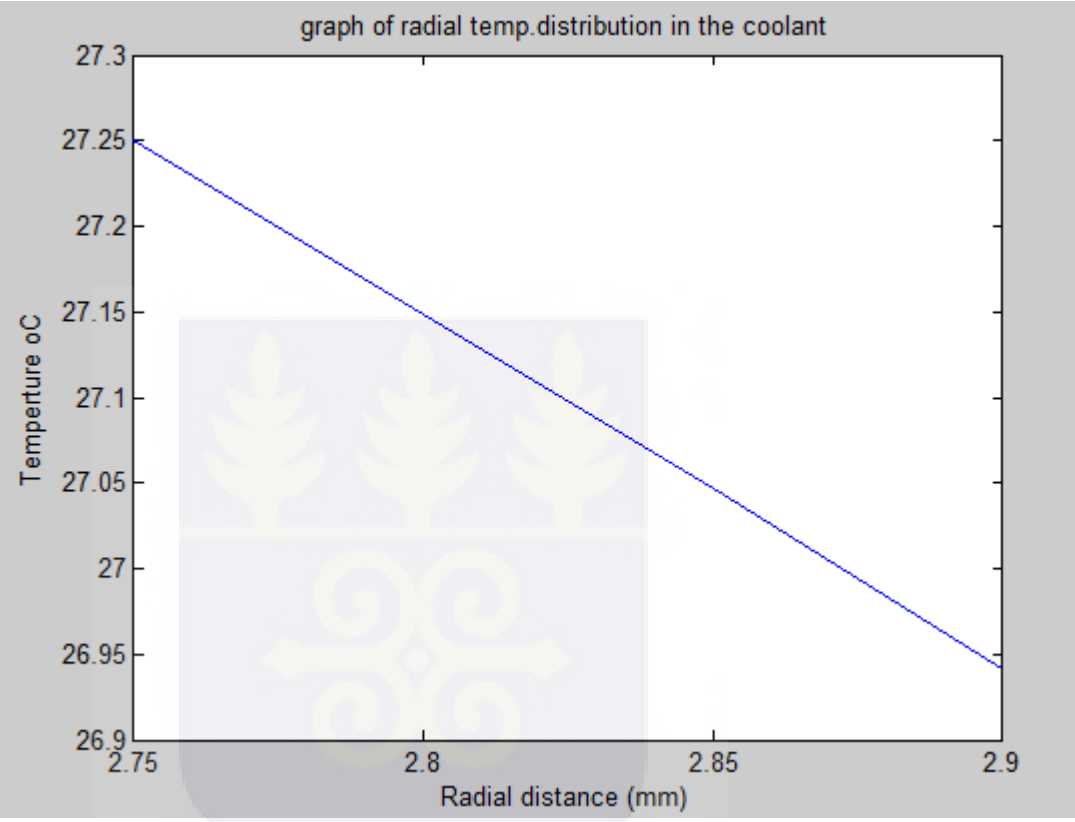

Fig.4.11. Radial temperature distribution in the coolant

Figure 4.12 is the combined plot of the temperature profile in the three components in the radial direction for the purposes of comparison and analysis.

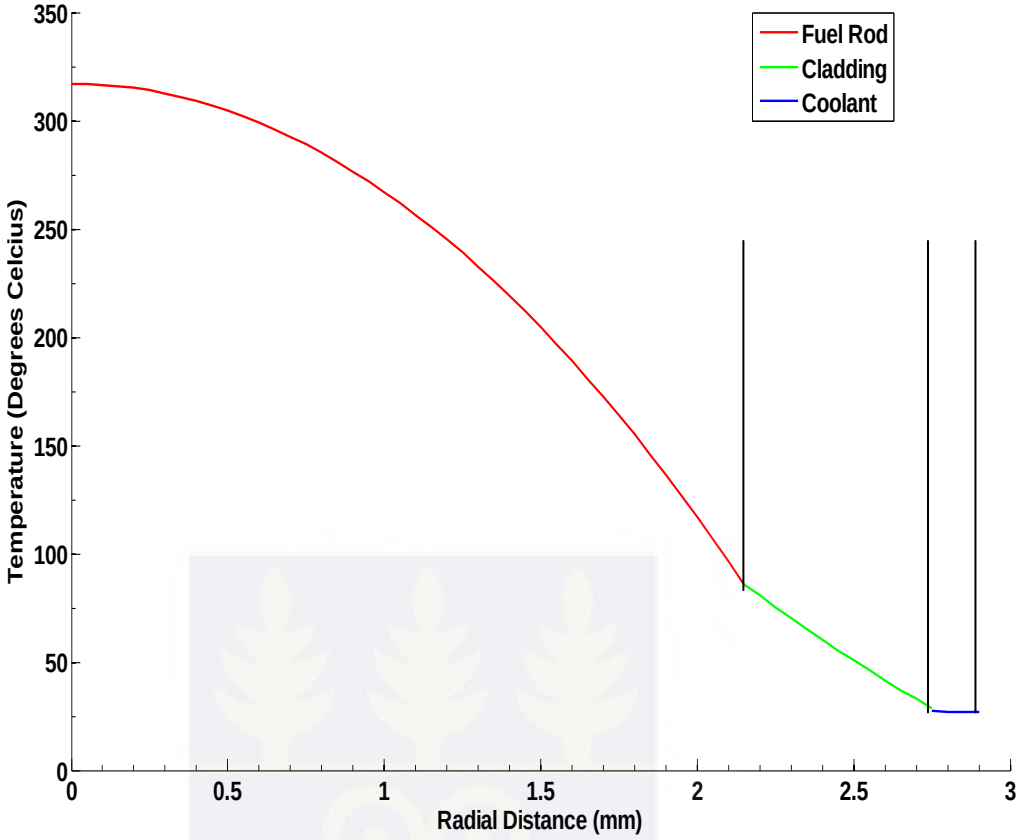

Fig.4.12. Combined radial temperature distribution in the fuel, cladding and coolant

4.5. Discussions

The maximum cladding temperature should be less than the maximum allowable temperature with a good safety margin. The maximum allowable temperature for zircaloy -4 cladding ranges from 380 ℃ to 400 ℃ [5].

By theory, since the location of the maximum temperature is given by an equation of the form: z_{max} = α arctan (b)

where b = γ or γ' or γ'' and $\gamma > \gamma' > \gamma''$, z_{max} increased as b increased and the maximum temperature drifted further downstream of the centerline of the channel.

Thus the location of the maximum temperature in the components was related to the thermal resistance and it shifted further downstream of the channel center as the resistance decreased.

4.5.1. Temperature distribution in the axial direction

The maximum temperature recorded at maximum channel power P_C =30 kW in the axial direction for fuel surface was 215 ℃. This occurred in the fuel center and was within the specification.

The coolant temperature increased continuously from the inlet of 24.5 ℃ to the exit value of 70.0 ℃. However the increase in temperature decreased as the exit point was approached a phenomenon which underpinned a safety condition and indicated effective cooling by natural condition.

Furthermore, a more efficient heat transfer was observed in the outer surface of the cladding, fuel surface and fuel center, where the temperature increased continuously along the channel in the region below the mid-point and reached a maximum value in each component in the upper half of the fuel channel in the order as shown in Table 4.3.

The temperature of the fuel center, the hottest part of the reactor, reached maximum point first then decreased in temperature after this point and was fastest considering the other two components, a design in support of safety condition.

The next maximum point was in the fuel which also began to decrease at a faster rate thereafter.

Finally, the temperature in the surface of cladding attained its maximum and decreased very quickly to the exit. The data in table 4.2 and figures 4.5, 4.6 and 4.7 were in support of these conclusions.

4.5.2. Temperature distribution in the radial direction

(i) Radial temperature distribution in the fuel

The temperature increased continuously from the fuel surface to the fuel center. For a fuel surface temperature of 86.00 ℃, the temperature along the center could increase to 317.13 ℃ an increase of 231.13 ℃ at a full operational power of 30 kW. However, the increase in temperature was not a steady one but decreased continuously between successive discrete points to the fuel center. Considering a space step size of 0.05 mm for the range ($0.05 \leq r \leq 2.15$ mm) on the radial distance axis, the decrease in temperature in degrees Celsius followed the sequence:

0.13, 0.37, 0.63, 0.87, 1.13, 1.37, 1.63, 1.87, 2.13, . . . , 9.37, 9.63, 9.87, 10.13, 10.37, 10.63.

Thus the temperature gradient was steep close to the fuel surface and gradual as the fuel center was approached.

(ii) Radial temperature distribution in the sheath (cladding)

A decrease in temperature from the inner to the outer surface of the cladding was obtained. The decrease increased towards the outer surface. The decrease in temperature in degrees Celsius for the clad thickness r ($2.15 \text{ mm} \leq r \leq 2.75$ mm) followed the sequence described by:

4.28, 4.36, 4.44, 4.54, 4.62, 4.71, 4.81, 4.91, 5.02, 5.13, 5.25, 5.36.

(iii) Radial temperature distribution in the coolant

In the coolant, the radial temperature decreased as expected as the coolant flowed away from the outer surface of the cladding. The decrease in temperature corrected to one decimal place was approximately 0.1 ℃, a constant, as shown by the sequence:

0.1009, 0.1027, 0.1046, 0.1063, 0.1082

CHAPTER FIVE

CONCLUSIONS AND RECOMMENDATIONS

5.1. Conclusions

The temperature profile in the channel of fuel assembly of MNSR has been simulated using LabVIEW software and the temperature distribution was validated by MATLAB and Excel software programs developed .

The temperature profile in the radial direction revealed that the coolant temperature increased continuously from the inlet value of 24.5℃ to the exit value of 70.0 ℃. In the outer surface of the cladding, the surface of the fuel and the fuel center components, the temperatures rose along the channel and reached maximum values above the centerline of the fuel channel as shown in Figure 5.1 [17].

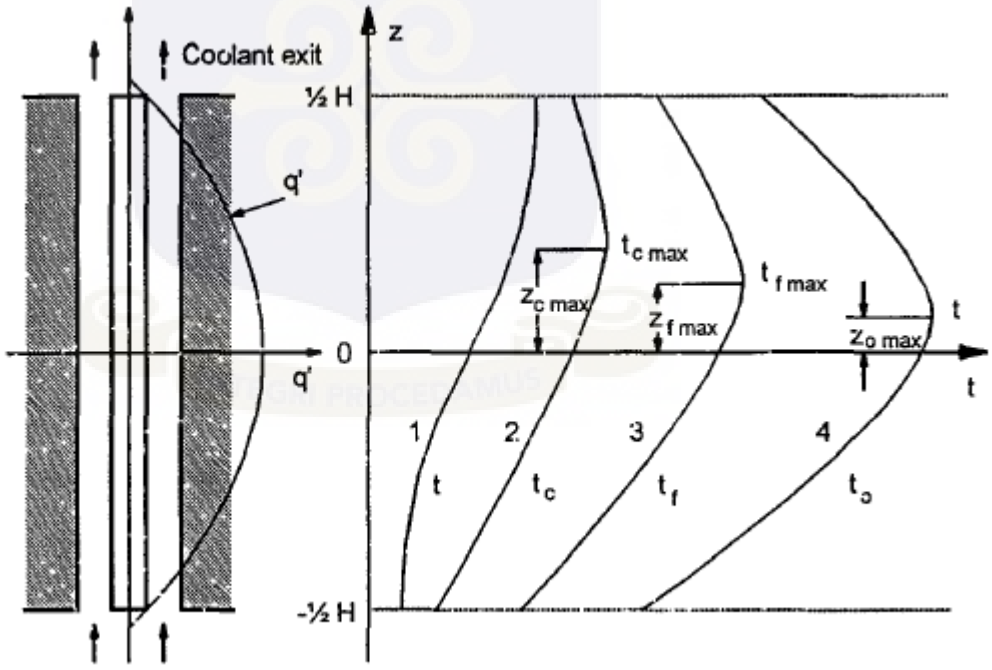

Fig 5.1 The axial temperature distribution in the fuel channel:

1. Coolant

2. Outer surface of the cladding

3. Fuel surface and

4. Fuel center.

On reaching the maximum temperatures, the temperatures in each of the other three zones continued to decrease to the exit of the fuel channel because the linear power after the maximum point began to drop more rapidly than the increase of coolant temperature.

Moving away from fuel center the maximum temperature shifted towards the exit of fuel channel (fig 5.1), mainly due to thermal resistance between the outside surface of the cladding and the coolant, in the cladding, in the gap region and in the fuel which decreased as one moved away from the fuel center.

In a good agreement, the LabVIEW simulation revealed that increasing the convective heat transfer coefficient, h_c, or decreasing the coolant mass flow rate, $\acute{m}$, shifted the point of maximum cladding temperature further away from the fuel channel mid-plane or centerline.

A detailed knowledge of the temperatures of the cladding and fuel center was important since together with critical heat flux, the temperature imposed limitations on the maximum allowable heat generation in the fuel element.

The changes in the temperature distribution in the radial direction were more significant than in the axial direction. Although the coolant temperature was 28℃, the maximum temperature at the fuel center exceeded 317 ℃ in the radial direction.

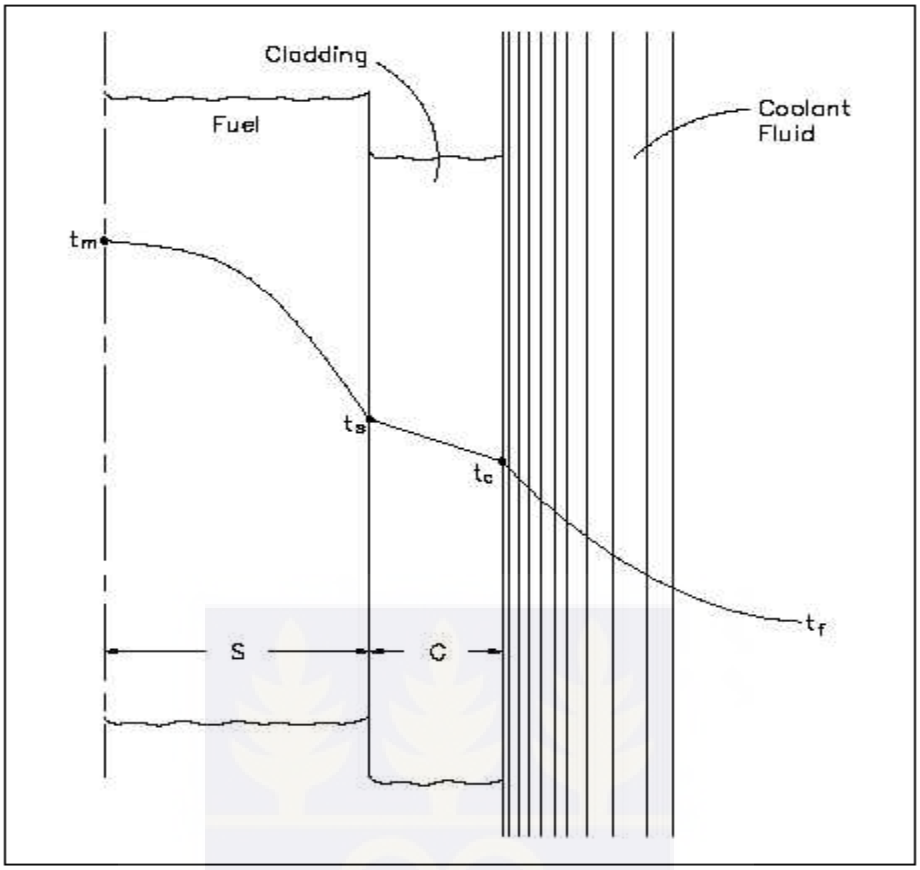

Figure 5.2 Radial Temperature Profile across a Fuel Rod and Coolant Channel.

The temperature distributions were skewed by the changing capacity of the coolant to remove the heat energy. Since the coolant increased in temperature as it flowed up the channel, the fuel cladding and the fuel temperatures were higher in the upper axial region of the core. A radial temperature profile across a reactor core (assuming all channel coolant flows are equal) followed the radial power distribution.

The areas with the highest heat generation rate (power) produced the most heat and had the highest temperatures.

A radial temperature profile for an individual fuel rod and coolant channel is shown in figure 5.2 [19].

The shapes of the temperature profiles were dependent upon the heat transfer coefficient of the various materials involved. The analysis on a single fuel rod can be easily extended to a multi-rod fuel bundle once there is a strong mixing existing between the laterally interconnected sub-channels bounded by the fuel rods or by the fuel rods and the channel wall. However, the position of the fuel rod in the entire fuel channel assembly will vary temperature values. The closer the fuel rod is to the center of the core the higher the temperature value.

LabVIEW has been used as a development environment and as generic graphical user interface because LabVIEW is based on a graphical language which is user friendly, can provide excellent graphics capabilities and in addition has the ability to make all results available and in real time.

5.2. Recommendations

The thesis presented an effective and a high quality LabVIEW simulations to execute on PC, the temperature profile in the channels of MNSR core so as to provide immediate access to knowledge on the temperature distribution in reactor core to nuclear personnel (mostly students) for familiarization, design evaluation, training and early guide to commissioning and operating procedures.

It is recommended that countries which are either aware of nuclear power or nuclear power ready in sharing this experience with interested parties, should develop various levels of training programs using LabVIEW and other simulation tools.

In the process of working together, the goals of self-reliance and the transfer of necessary nuclear reactor knowledge will be obtained which will help to fulfill the objectives of the nuclear human resource development initiatives.

The simulation was carried out on nuclear reactor of cylindrical geometry. It can be demonstrated on other geometries to compare the efficiency of heat transfer.

Future work will focus on including additional interactive features for operator actions as well as extending the development to AP 1000 reactor design.

REFERENCES

[1] Fenech, H (Editor), Heat Transfer and fluid flow in Nuclear Systems, Pergamon Press, University of California , USA ,1981.

[2] Tong L.S., Heat Transfer in water cooled nuclear reactors, Nuclear Eng. and Design, Vol. 6, 1967.

[3] Galliland, E. R. The Science and Engineering of Nuclear Reactors, Academic Press, San Diego, CA, USA, 1949

[4] Kampf, H and Karsten, G., Table of Parameters, Nuclear Application Vol. 9, 1970.

[5] Ogawa ,S.Y., Lees, E.A. and Lyons, M.F., Power Reactor High Perfomance U Program Fuel Design Summary and Program Status, GEAP-5591 Pergamon Press Inc New York,1968.

[6] Ross, A.M. and Stoute, R.L., Heat Transfer Coefficient Between U02 and Zircaloy-2, AECL-1552, John Wiley & Sons Inc. New York, 1962.

[7] Lyons, F.M. et al. UOz P'owder and Pellet Thermal Conductivity During Irradiation,

GEAP-SIOO-l, Harwood Academic Publishers, New York, 1966

[8] Cetinkale, T.K. and Fishenden , M., Thermal Conductance of Metal Surfaces in Contact, Proc. General Discussion on Heat Transfer, Institute of Mechanical Engineers, London. UK, 1951.

[9] Godfrey, T.G., Fulkerson, W., Kollie, T.G., Moore, J.P and McElroy, D.L., Thermal Conductvity of Uranium Dioxide and Armco Iron by an Improved Radial Flow Technique, ORNL -3556. Oak Ridge National Laboratory, USA, 1964.

[10] Kenard F.K., Kinetic Theory of Gases, 1st Edition, McGraw-Hill Book Company,New York, pp.311-325, 1938.

[11] Sonntag. R.E. and Van Wylen, GJ. Introduction to Thermodynamics - Classical and Statistical 3rd. Edition, John Willey & Sons New York, pp. 197-198, 1991

[12] May, J.F., Notley, M.J.F., Stoute, R.L. Rcb~rtson, A L. Observation on Thermal Conductivity of Uranium Dioxide, AECL-1641, Atomic Energy of Canada Limited, Quebec, 1962.

[13] Akaho E.H.K., Maakuu B.T., Anim-Sampong S., Emi-Reynolds G., Boadu H.O., Osae E.K., Akoto Bamford S., Dodoo-Amoo D.N.A., Ghana Research Reactor-1 GAEC-NNRI-RT-90 Final Safety Analysis Report, Accra, November,2003.

[14] National Instruments, 2003. LabVIEW: Getting Started with LabVIEW

[15] Shiralkar M., LabVIEW Graphical Programming Course, A Technical Review , National Academy Press, Washington, 2010.

http:/cnx.org/content/coll0241/1.4/Retrieved: August 2012.

[16] Korsah K., Computational Methods in Reactor Dynamics: Modeling, Simulation and Control in LabVIEW, Unpublished Manual, University of Ghana, School of Nuclear and Allied Sciences, Accra, 2012

[17] Jeff C.B., Introduction to Nuclear Science. University of Wisconsin-La Crosse, USA. July,15, 2008.

[18] Robeltson, J.AL. $\int kde$ in Fuel Irradiations, AECL-807,Hemisphere Publishing Corporation, New York 1959.

[19] MacDonald, P.E., Thompson, L.D. MATPRO-Handbook of Material Properties for use in Analysis of L Light Water Reactor Fuel Rod Behavior, Idaho Nuclear Engineering Laboratory, Idaho, USA, 1976.

[20] Wm. J. Garland, Professor, Fuel - Coolant Heat Transfer, McMaster University, Department of Engineering Physics ,Hamilton, Ontario, Canada,2008.

[21] Owen C , Nuclear Reactor Safety Heat Transfer, Hemisphere publishing Co-operation , University of Michigan , Michigan 18 Dec, 2006.